Supporting Information

Supracluster Assembly of Al_4 Precursor toward Enhanced Optical Property Study

Fan Yang,‡[a,b] Rui-Yan Chen,‡[a,c], San-Tai Wang,[a,b] Yan-Ping He [a,*], Wei-Hui Fang [a,b*] and Jian Zhang [a]

[a] State Key Laboratory of Structural Chemistry, Fujian Institute of Research on the Structure of Matter, Chinese Academy of Sciences, Fuzhou, Fujian 350002, P. R. China. E-mail: hyp041@163.com, and fwh@fjirsm.ac.cn

[b] University of Chinese Academy of Sciences, Beijing 100049, P. R. China

[c] MOE Key Laboratory of Cluster Science, School of Chemistry and Chemical Engineering, Beijing Institute of Technology, Beijing 100081, China

‡ These authors contributed equally to this work.

Table of Content

1. Experimental Section.

Chemicals and Materials. All the reagents and solvents employed are purchased commercially and used as received without further purification. $Al(O^iPr)_3$, 2,3-dihydroxybenzoic (H_3L), pyrazole, silver perchlorate ($AgClO_4$), (R)-2,2‘-bis(diphenylphosphino)-1,1‘- binaphthyl (R-binap), (S)-2,2‘-bis(diphenylphosphino)-1,1‘-binaphthyl (S-binap) were acquired from Aladdin Chemical Reagent Shaihai. N,N-Dimethylformamide (DMF), ethanol (≥99.5 %), formamide (CH_3ON), ammonium hydroxide, iron (II) sulfate heptahydrate ($FeSO_4·7H_2O$) were bought from Sinopharm Chemical Reagent Beijing. Copper(I) oxide (Cu_2O), bis(diphenylphosphino)methane (bdpm), 1,3-bis(diphenylphosphino)propane (1,3-bdpp), 1,4-bis(diphenylphosphino)butane (1,4-bdpb), 1,5-bis(diphenylphosphino)pentane (1,5-bdpp), 2,9-dimethyl-4,7-diphenyl-1,10-phenanthroline (dmdpp), (oxydi-2,1-phenylene)bis(diphenylphosphine) (DPEphos), 1,10-phenanthroline monohydrate (phen), 3,4,7,8-tetramethyl-1,10-phenanthroline (me_4phen) were purchased from Adamas-beta.

Materials and Instrumentation. The energy dispersive spectroscopy (EDS) analyses of single crystals were performed on a JEOL JSM6700F field-emission scanning electron microscope equipped with an Oxford INCA system. IR spectra (KBr pellets) were recorded on an ABB Bomem MB102 spectrometer over a range 400-3900 cm^{-1}. Powder X-ray diffraction (PXRD) data were collected on a Rigaku Mini Flex II diffractometer using Ga Kα radiation (λ = 1.3405 Å) under ambient conditions. The UV-vis diffuse reflection data were recorded at room temperature using a powder sample with $BaSO_4$ as a standard (100% reflectance) on a PerkinElmer Lamda-950 UV spectrophotometer and scanned at 200-1200 nm. The absorption data were calculated from the Kubelka-Munk function, ($F(R) = (1-R)^2/2R$), where R representing the reflectance. The TGA curves were recorded in the region of 20–800 °C using a heating rate of 10 °C min^{-1} in a flowing N_2 atmosphere on a Mettler Toledo TGA/SDTA 851e analyser. The liquid CD spectra were measured on an MOS-450 spectropolarimeter using methyl alcohol and cuvet. The PL spectra were finished on the UV/V/NIR Fluorescence Spectrometer (Edinburgh, FLS1000).

General methods for X-ray Crystallography. Crystallographic data for compounds (**AlOC-168** to **AlOC-176**) were collected on Hybrid Pixel Array detector equipped with graphite-monochromated Ga K*α* radiation (λ = 1.3405 Å). The structures were solved with direct methods using OLEX^2 and refined by full-matrix least-squares on F^2 using *SHELXTL*. Contributions to scattering due to disordered solvent molecules were removed using the *SQUEEZE* routine of *PLATON*. All hydrogen atoms were theoretical hydrogenation, riding on the concerned atoms and refined with fixed thermal factors. Non-hydrogen atoms were refined anisotropically.

The synthesis of Al_4 precursor.

The synthesis of $(Me_2NH_2)_4[Al_4(L)_4(Cat)_2]$ (AlOC-13). According to our previous work: Inorg. Chem. 2020, 59, 13760−13766. A mixture of $Al(O^iPr)_3$ (0.2 g, 0.98 mmol), 2,3-dihydroxybenzoic acid (H_3L, 0.4 g, 2.60 mmol), pyrazole (2 g, 29.38 mmol), and DMF (5 mL) was sealed in a 25 mL Teflon reactor and transferred to a preheated oven at 160 °C for 3 days. When cooled to room temperature, light brown crystals of **AlOC-13** were obtained (yield: 75 % based on $Al(O^iPr)_3$). Synthesis scale up is also possible, using the 25 mL Teflon reactor can obtain 0.27 g **AlOC-13**, and using the 50 mL Teflon reactor can obtain 0.68 g **AlOC-13.**

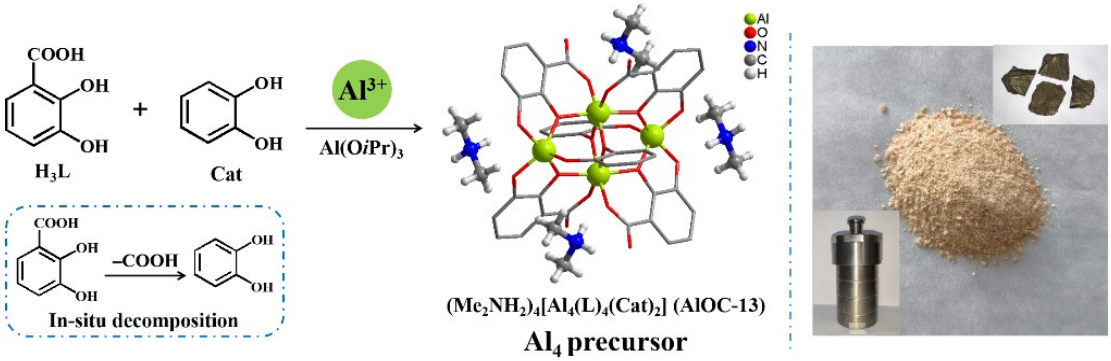

Scheme S1. The synthesis scheme of Al_4 precursor and its crystal and powder photos.

Supracluster assembly tructures via non-covalent bonds:

Solvothermal synthesis of AlOC-168 $(Me_2NH_2)_3[Ag(1,3\text{-}bdpp)_2][Al_4(L)_4(Cat)_2]\cdot$*Guests*. In a 20 mL vial, Al_4 precursor (55 mg, 0.05 mmol) was dissolved in 2 mL of H_2O at 100 °C for 6 h. The mixture of 2 mL precursor, silver perchlorate ($AgClO_4$, 14 mg, 0.07 mmol), 1,3-bis(diphenylphosphino)propane (1,3-bdpp, 45 mg, 0.11 mmol), EtOH (2 mL), DMF (2 mL) was sealed in a 20 mL vial at 80 °C for 24 h. When cooled to room temperature, light brown crystals were obtained.

(yield: 75 % based on Al_4 precursor). The crystals are rinsed with EtOH and preserved under a sealed and dry environment.

Solvothermal synthesis of AlOC-169 $(Me_2NH_2)_3[Ag(dmdpp)(DPEphos)][Al_4(L)_4(Cat)_2]\cdot$*Guests*. In a 20 mL vial, Al_4 precursor (55 mg, 0.05 mmol) was dissolved in 2 mL of H_2O at 100 °C for 6 h. The mixture of 2 mL precursor, silver perchlorate ($AgClO_4$, 9 mg, 0.04 mmol), 2,9-dimethyl-4,7-diphenyl-1,10-phenanthroline (dmdpp, 15 mg, 0.04 mmol), (oxydi-2,1-phenylene)bis(diphenylphosphine) (DPEphos, 22 mg, 0.04 mmol), EtOH (2 mL), DMF (2 mL) was sealed in a 20 mL vial at 80 °C for 24 h. When cooled to room temperature, light yellow crystals were obtained. (yield: 70 % based on precursor). The crystals are rinsed with EtOH and preserved under a sealed and dry environment.

Solvothermal synthesis of AlOC-170(R) $(Me_2NH_2)_6[Ag(R\text{-}binap)_2]_2[Al_4(L)_4(Cat)_2]_2\cdot$*Guests*. In a 20 mL vial, Al_4 precursor (55 mg, 0.05 mmol) was dissolved in 2 mL of H_2O at 100 °C for 6 h. The mixture of 2 mL precursor, silver perchlorate ($AgClO_4$, 30 mg, 0.15 mmol), (R)-2,2‘-bis(diphenylphosphino)-1,1‘-binaphthyl (R-binap, 97 mg, 0.16 mmol), EtOH (2 mL), DMF (2 mL) was sealed in a 20 mL vial at 80 °C for 24 h. When cooled to room temperature, colourless crystals were obtained. (yield: 35 % based on precursor). The crystals are rinsed with EtOH and preserved under a sealed and dry environment.

Solvothermal synthesis of AlOC-170(S) $(Me_2NH_2)_6[Ag(S\text{-}binap)_2]_2[Al_4(L)_4(Cat)_2]_2\cdot$*Guests*. In a 20 mL vial, Al_4 precursor (55 mg, 0.05 mmol) was dissolved in 2 mL of H_2O at 100 °C for 6 h. The mixture of 2 mL precursor, silver perchlorate ($AgClO_4$, 30 mg, 0.15 mmol), (S)-2,2‘-bis(diphenylphosphino)-1,1‘-binaphthyl (S-binap, 97 mg, 0.16 mmol), EtOH (2 mL), DMF (2mL) was sealed in a 20 mL vial at 80 °C for 24 h. When cooled to room temperature, colourless crystals were obtained. (yield: 35 % based on precursor). The crystals are rinsed with EtOH and preserved under a sealed and dry environment.

Solvothermal synthesis of AlOC-171 $[Fe(phen)_3]_2[Al_4(L)_4(Cat)_2]\cdot$*Guests*. In a 20 mL vial, Al_4 precursor (55 mg, 0.05 mmol) was dissolved in 2 mL of H_2O at 100 °C for 6 h. The mixture of 2 mL precursor, iron (II) sulfate heptahydrate ($FeSO_4\cdot 7H_2O$, 30 mg, 0.11 mmol), 1,10-phenanthroline monohydrate (phen, 30 mg, 0.15 mmol), DMF

(2mL), ammonium hydroxide (5 drops) was sealed in a 20 mL vial at 80 °C for 24 h. When cooled to room temperature, deep red crystals were obtained. (yield: 70 % based on precursor). The crystals are rinsed with DMF and preserved under a sealed and dry environment.

Solvothermal synthesis of AlOC-172 $[Cu(Me_4phen)_2(H_2O)]_2[Al_4(L)_4(Cat)_2]$·*Guests*. In a 20 mL vial, Al_4 precursor (55 mg, 0.05 mmol) was dissolved in 2 mL of H_2O at 100 °C for 6 h. The mixture of 2 mL precursor, copper(I) oxide (Cu_2O, 7 mg, 0.05 mmol), 3,4,7,8-tetramethyl-1,10-phenanthroline (me_4phen, 14 mg, 0.06 mmol), NMF (2 mL), ammonium hydroxide (5 drops) was sealed in a 20 mL vial at 80 °C for 24 h. When cooled to room temperature, grey crystals were obtained. (yield: 45 % based on precursor). The crystals are rinsed with DMF and preserved under a sealed and dry environment.

Supracluster assembly structures via coordination bonds

Solvothermal synthesis of AlOC-173 $[Ag_2(bdpm)_2]_2[Al_4(L)_4(Cat)_2]$·*Guests*. ~~In a 20 mL vial,~~ Al_4 precursor (55 mg, 0.05 mmol) was dissolved in 2 mL of H_2O at 100 °C for 6 h. The mixture of 2 mL precursor, silver perchlorate ($AgClO_4$, 34 mg, 0.16 mmol), bis(diphenylphosphino)methane (bdpm, 62 mg, 0.16 mmol), EtOH (2 mL), DMF (2 mL) was sealed in a 20 mL vial at 80 °C for 24 h. When cooled to room temperature, white crystals were obtained. (yield: 45 % based on precursor). The crystals are rinsed with EtOH and preserved under a sealed and dry environment.

Solvothermal synthesis of AlOC-174 $[Ag_3(1,5\text{-}bdpp)_3]_2[Al_4(L)_4(Cat)_2](ClO_4)_2$·*Guests*. ~~In a 20 mL vial,~~ Al_4 precursor (55 mg, 0.05 mmol) was dissolved in 2 mL of H_2O at 100°C for 6 h. The mixture of 2 mL precursor, silver perchlorate ($AgClO_4$, 51 mg, 0.25 mmol), 1,5-bis(diphenylphosphino)pentane (1,5-bdpp, 106 mg, 0.24 mmol), EtOH (2 mL), DMF (2 mL) was sealed in a 20 mL vial at 80 °C for 24 h. When cooled to room temperature, white crystals were obtained. (yield: 35 % based on precursor). The crystals are rinsed with EtOH and preserved under a sealed and dry environment.

Solvothermal synthesis of AlOC-175 $[Ag_4(1,4\text{-}bdpb)_3][Al_4(L)_4(Cat)_2]$·*Guests*. In a 20 mL vial, Al_4 precursor (55 mg, 0.05 mmol) was dissolved in 2 mL of H_2O at 100 °C for 6 h. The mixture of 2 mL precursor, silver perchlorate ($AgClO_4$, 30 mg, 0.15 mmol),

1,4-bis(diphenylphosphino)butane (1,4-bdpb, 60 mg, 0.14 mmol), ethanol (2 mL), DMF (2 mL) was sealed in a 20 mL vial at 80 °C for 24 h. When cooled to room temperature, light brown crystals were obtained. (yield: 55 % based on precursor). The crystals are rinsed with EtOH and preserved under a sealed and dry environment.

Solvothermal synthesis of AlOC-176 [Ag_4(bdpm)$_2$(1,4-bdpb)][Al_4(L)$_4$(Cat)$_2$]·*Guests*. In a 20 mL vial, Al_4 precursor (55 mg, 0.05 mmol) was dissolved in 2 mL of H_2O at 100 °C for 6 h. The mixture of 2 mL precursor, silver perchlorate ($AgClO_4$, 34 mg, 0.16 mmol), bis(diphenylphosphino)methane (bdpm, 31 mg, 0.08 mmol), 1,4-bis(diphenylphosphino)butane (1,4-bdpb, 34 mg, 0.08 mmol), EtOH (2 mL), DMF (2 mL) was sealed in a 20 mL vial at 80 °C for 24 h. When cooled to room temperature, light yellow crystals were obtained. (yield: 75 % based on precursor). The crystals are rinsed with EtOH and preserved under a sealed and dry environment.

Fabrication of Al_4 precursor@PDMS and AlOCs@PDMS.

Al_4 precursor@PDMS and AlOCs@PDMS were fabricated using Sylgard 184 (Dow Corning) by thoroughly mixing 10 parts base to 1 part curing agent. The coordinate crystals were mixed with the PDMS solution to form coordinates dispersed PDMS suspension. And then, the mixture suspension was added into a template and then put the template into a vacuum oven at 60 ℃ for 6 hours. Last, the transparent and flexible Al_4 precursor@PDMS and AlOCs@PDMS were obtained.

Z-scan measurements.

The third-order NLO properties of the sample were evaluated by using the Z-scan technique. The excitation light source was an Nd:YAG laser with a repetiton rate of 5 Hz. The laser pulse (period, 5 ns; wavelength, 532 nm) was split into two beams with a mirror. The pulse energies at the front and back of the samples were monitored using energy detectors 1 and 2. All of the measurements wre conducted at room temperature. The sample was mounted on a computer-controlled translation stage that shifted each sample along the z-axis.

Calculation of the nonlinear optical parameters.

The imaginary parts of the third-order susceptibility *Im* $\chi^{(3)}$ was determined by the following equation:

$$Im\,\chi^{(3)}(esu) = \frac{c\left(m/s\right)^2\beta(m/W){n_0}^2}{240\pi^2\omega(s^{-1})}$$

Where *β* is the nonlinear absorption coefficient, *c* is the speed of ligtht in vacuum, *ω* is angular frequency of the incident wavelength and n_0 is the linear refractive index, respectively.

The relationship of the transmittance and input laser intensity for a spatially Gaussian beam can be plotted from the open-operture Z-scan curve. From the input laser pulse energy E_{in} and beam radius $\omega(z)$, the light fluence $F_{in}(z)$ at any position can be obtained. $F_{in}(z)$ is defined as:

$$F_{in}(z) = \frac{4E_{in}\sqrt{\ln 2}}{\pi^{\frac{3}{2}}\omega(z)^2}$$

Where $\omega(z)$ is defined as:

$$\omega(z) = \omega_0\left[1 + \left(\frac{z}{z_0}\right)^2\right]^{\frac{1}{2}}$$

where ω_0 and z_0 are the light beam radius and the Rayleigh range, respectively, and z_0 is defined as:

$$z_0 = \frac{k{\omega_0}^2}{2}$$

where *k* is defined as:

$$k = \frac{2\pi}{\lambda}$$

The curve of output fluence versus input fluence in Figure 3b was plotted from Figure 3c.

The equation fits for the nonlinear absorption coefficient *β* as follows:

$$T(Z,S=1) = \frac{1}{\sqrt{\pi}q_0(Z,0)}\int_{-\infty}^{\infty} Ln\left[1 + q_0(Z,0)e^{(-r)^2}\right]dr$$

$$q_0(Z,0) = \beta I_0 L_{eff}$$

$$L_{eff} = \frac{1 - e^{-\alpha l}}{\alpha}$$

In these equations, I_0 is the on-axis peak intensity at the focus (Z=0), L_{eff} is the effective thickness of the sample, α is the linear absorption coefficient, and l is the sample thickness.

Table S1. Crystallographic Data and Structure Refinement Details for Compounds **AIOC-168** to **AIOC-170(S)**.

compound	**AIOC-168**	**AIOC-169**	**AIOC-170(R)**	**AIOC-170(S)**
CCDC	2303391	2303392	2303393	2303394
formula	$C_{100}H_{100}AgAl_4N_3O_{22}P_4$	$C_{106}H_{85}AgAl_4N_4O_{21}P_2$	$C_{268}H_{207}Ag_2Al_8N_3O_{44}P_8$	$C_{267}H_{207}Ag_2Al_8N_5O_{39}P_8$
formula weight	2036.50	2028.51	4846.64	4788.70
crystal system	Triclinic	Orthorhombic	Monoclinic	Monoclinic
space group	*P*-1	*Pbca*	$P2_1$	$P2_1$
a (Å)	12.9543(2)	22.2866(13)	22.7099(4)	22.7861(5)
b (Å)	19.4350(3)	22.3784(8)	22.9468(4)	23.1721(4)
c (Å)	20.0165(3)	43.3645(19)	22.7802(4)	23.0114(4)
α (°)	95.8910(10)	90	90	90
β (°)	93.4480(10)	90	93.312(2)	93.565(2)
γ (°)	108.1350(10)	90	90	90
V (Å^3)	4741.21(13)	21627.5(18)	11851.4(4)	12126.5(4)
Z	2	8	2	2
D_{calcd} (g cm^{-3})	1.427	1.246	1.358	1.311
μ(Ga K*a*) (mm^{-1})	2.214	1.761	1.833	1.776
F(000)	2114.0	8368.0	5003.0	4948.0
temperature (K)	99.9(4)	293(2)	100.0(3)	293.00(10)
theta min, max (deg)	3.876, 120.204	4.944, 85.238	4.644, 85.038	4.71, 105.856
GOF	1.051	1.439	1.023	1.043
R (int)	0.0482	0.1286	0.0733	0.0453
observed data [(*I* > 2*σ*(*I*)]	20749	10359	18350	24232
R_1, wR_2 (all data)[a]	0.0709, 0.1361	0.1615, 0.3777	0.0940, 0.2193	0.0717, 0.1498
Min and max resd dens (e·Å^{-3})	-0.95, 1.11	-1.26, 2.73	-1.12, 1.86	-1.07, 0.56
Flack	------	------	-0.022(8)	0.005(7)

Table S2. Crystallographic Data and Structure Refinement Details for Compounds **AIOC-171** to **AIOC-174.**

compound	**AIOC-171**	**AIOC-172**	**AIOC-173**	**AIOC-174**
CCDC	2303395	2303396	2303397	2303398
formula	$C_{112}H_{72}Al_4Fe_2N_{12}O_{22}$	$C_{106}H_{94}Al_4Cu_2N_{10}O_{24}$	$C_{140}H_{108}Ag_4Al_4O_{20}P_8$	$C_{220}H_{214}Ag_6Al_4Cl_2N_2O_{30}P_{12}$
formula weight	2157.43	2126.91	2897.42	4563.60
crystal system	Monoclinic	Triclinic	Triclinic	Triclinic
space group	*I*2/*a*	*P*-1	*P*-1	*P*-1
a (Å)	29.3776(9)	12.5246(3)	14.6487(3)	17.2507(2)
b (Å)	11.8729(2)	13.3926(4)	15.1376(3)	18.2402(3)
c (Å)	30.2151(9)	15.6926(5)	17.0263(3)	19.1425(3)
α (°)	90	114.226(3)	96.706(2)	66.449(2)
β (°)	117.862(4)	91.865(2)	112.108(2)	72.9580(10)
γ (°)	90	100.748(2)	98.931(2)	69.9380(10)
V (Å^3)	9317.2(5)	2340.77(13)	3391.61(12)	5100.72(15)
Z	4	1	1	1
D_{calcd} (g cm^{-3})	1.538	1.509	1.419	1.486
μ(Ga K*a*) (mm^{-1})	2.435	3.143	4.132	4.241
F(000)	4432.0	1102.0	1468.0	2336.0
temperature (K)	293(2)	100.00(10)	100.00(10)	100.00(10)
theta min, max (deg)	5.752, 85.284	5.41, 107.702	4.962, 107.708	4.756, 107.71
GOF	1.051	1.020	0.917	1.008
R (int)	0.0283	0.0624	0.0711	0.0656
observed data [($I > 2\sigma(I)$]	4937	8510	12066	18515
R_1, wR_2 (all data)[a]	0.0481, 0.1079	0.0596, 0.1402	0.0635, 0.1709	0.0473, 0.1161
Min and max resd dens (e·Å^{-3})	-0.28, 0.25	-0.72, 0.92	-1.75, 1.75	-1.20, 2.01

Table S3. Crystallographic Data and Structure Refinement Details for Compounds **AlOC-175** to **AlOC-176.**

compound	**AlOC-175**	**AlOC-176**
CCDC	2303398	2303400
formula	$C_{62}H_{52}Ag_2Al_2O_{10}P_3$	$C_{61}H_{54}Ag_2Al_2NO_{10}P_3$
formula weight	1319.64	1323.66
crystal system	Monoclinic	Triclinic
space group	*I*2/*a*	*P*-1
a (Å)	19.0898(2)	13.99610(10)
b (Å)	19.1937(2)	15.35070(10)
c (Å)	30.3739(2)	15.96420(10)
α (°)	90	113.0180(10)
β (°)	93.8530(10)	91.0680(10)
γ (°)	90	114.7720(10)
V (Å^3)	11103.96(18)	2797.17(4)
Z	8	2
D_{calcd} (g cm^{-3})	1.579	1.572
μ(Ga K*a*) (mm^{-1})	4.918	4.885
F(000)	5352.0	1344.0
temperature (K)	100.0(2)	100.0(2)
theta min, max (deg)	5.07, 120.534	5.358, 120.46
GOF	1.026	1.065
R (int)	0.0330	0.0309
observed data [($I > 2\sigma(I)$]	12352	12467
R_1, wR_2 (all data)[a]	0.0401, 0.0994	0.0492, 0.1056
Min and max resd dens (e·Å^{-3})	-0.75, 0.28	-1.65, 1.70

2. The detailed structure information of AlOC-168 to AlOC-176.

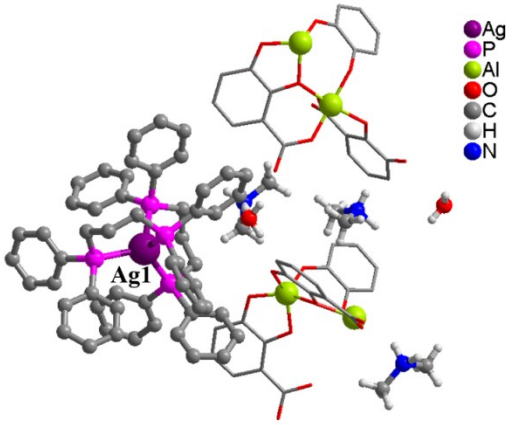

Figure S1. The asymmetric unit of **AlOC-168**, showing one Al_4 cluster, one $[Ag(1,3\text{-}bdpp)_2]^+$ unit and three $(Me_2NH_2)^+$ cations, and two H_2O molecules (Other solvents could not be located because of high disorder).

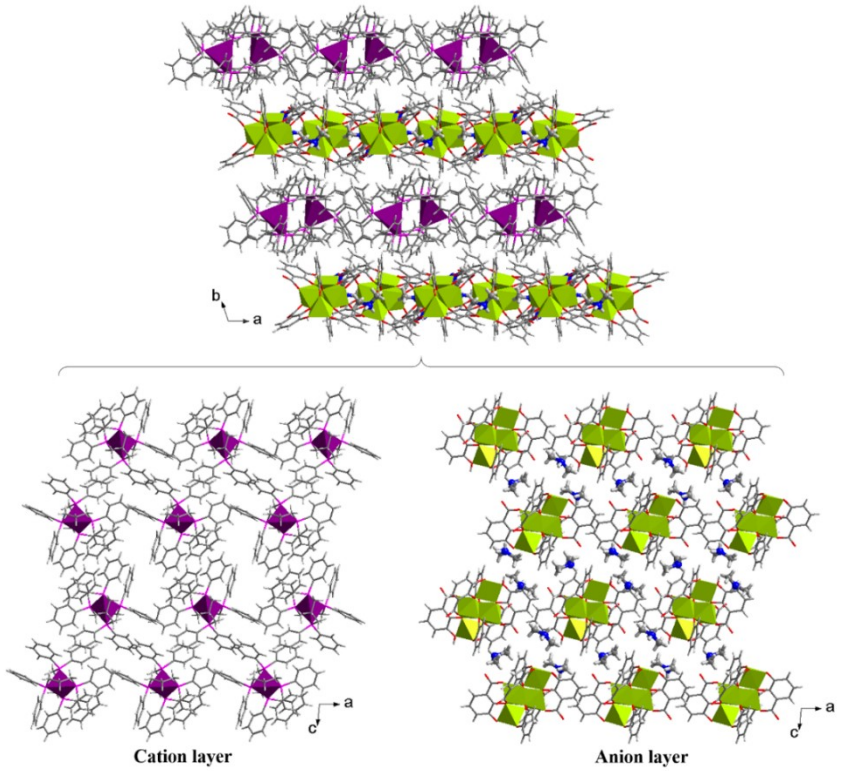

Figure S2. The packed structure along the c-axis composed of a cationic $[Ag(1,3\text{-}bdpp)_2]^+$ layer and an anionic Al_4 layer in **AlOC-168**, in which the $(Me_2NH_2)^+$ countercations are located in the anion layer.

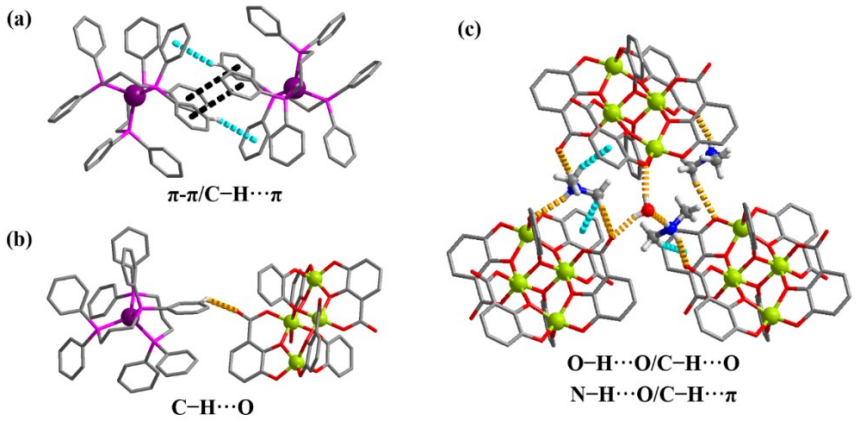

Figure S3. The supramolecular interactions in **AlOC-168**.

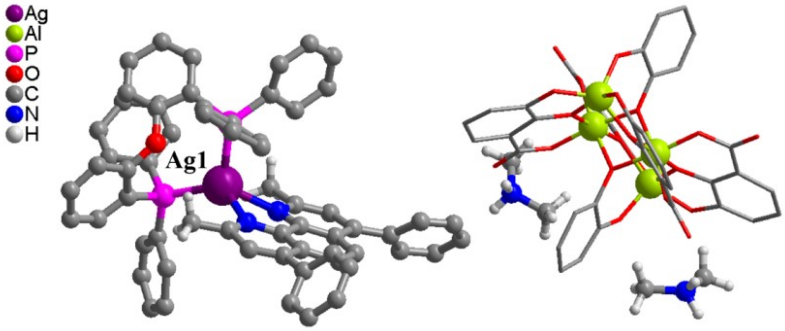

Figure S4. The asymmetric unit of **AlOC-169**, showing one Al_4 cluster, one $[Ag(dmdpp)(DPEphos)]^+$ unit, and two $(Me_2NH_2)^+$ cations (Other $(Me_2NH_2)^+$ cation and solvent molecules could not be located because of high disorder).

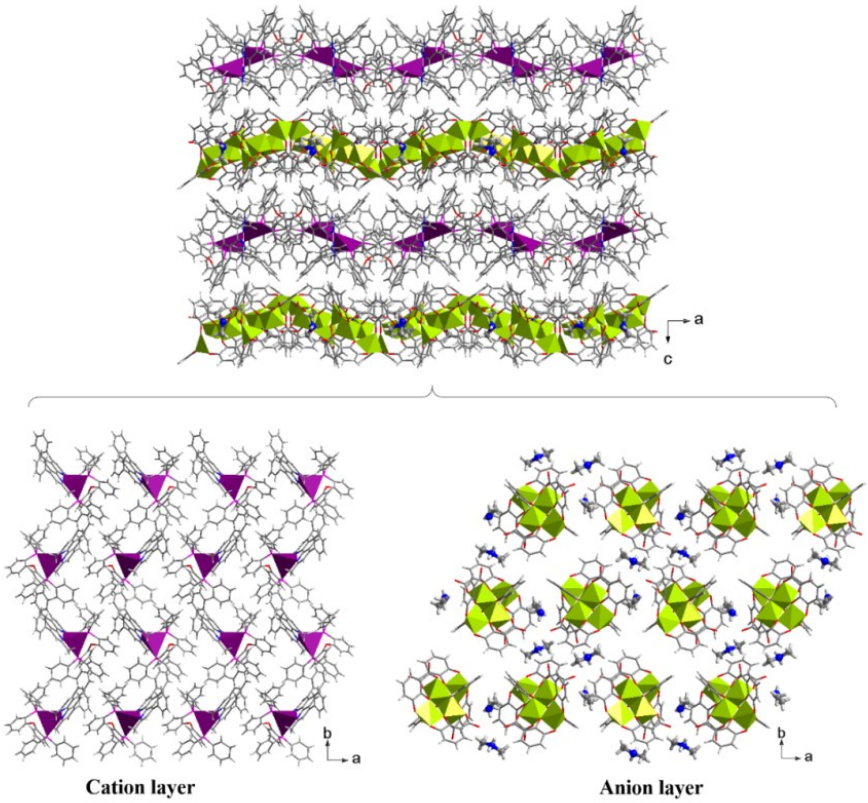

Figure S5. The packed structure along the b-axis composed of cationic $[Ag(dmdpp)(DPEphos)]^+$ layer and anionic Al_4 layer in **AlOC-169**, in which the $(Me_2NH_2)^+$ countercations are located in the anion layer.

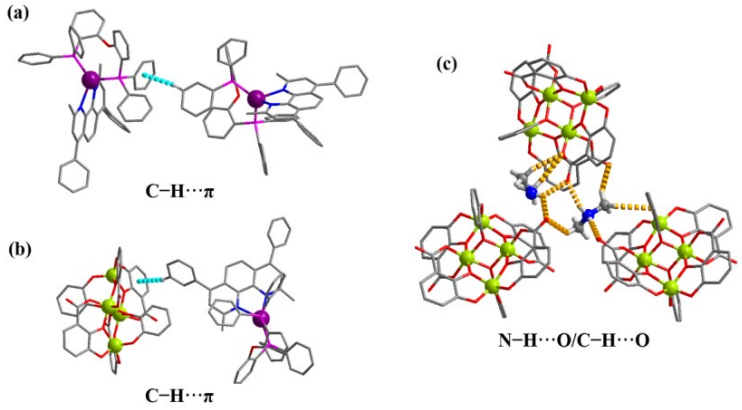

Figure S6. The supramolecular interactions in **AlOC-169**.

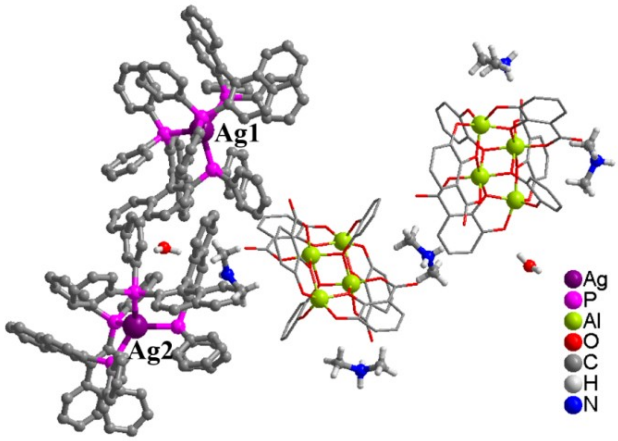

Figure S7. The asymmetric unit of **AlOC-170(R)**, showing two Al_4 clusters, two $[Ag(R\text{-}binap)_2]^+$ units, five $(Me_2NH_2)^+$ cations, and two H_2O molecules. (Other $(Me_2NH_2)^+$ cation and solvent molecules could not be located because of high disorder).

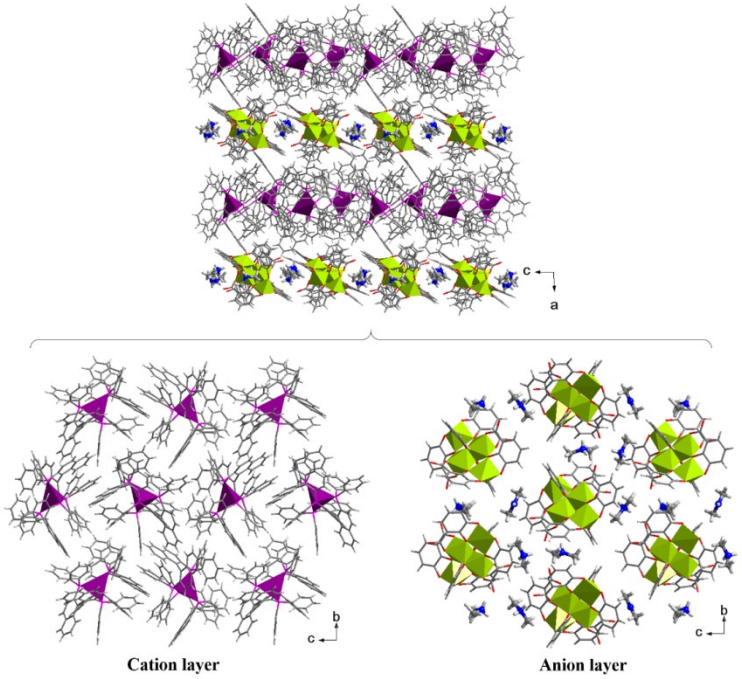

Figure S8. The packed structure along the b-axis composed of cationic $[Ag(R\text{-}binap)_2]^+$ layer and anionic Al_4 layer in **AlOC-170(R)**, in which the $(Me_2NH_2)^+$ countercations are located in the anion layer.

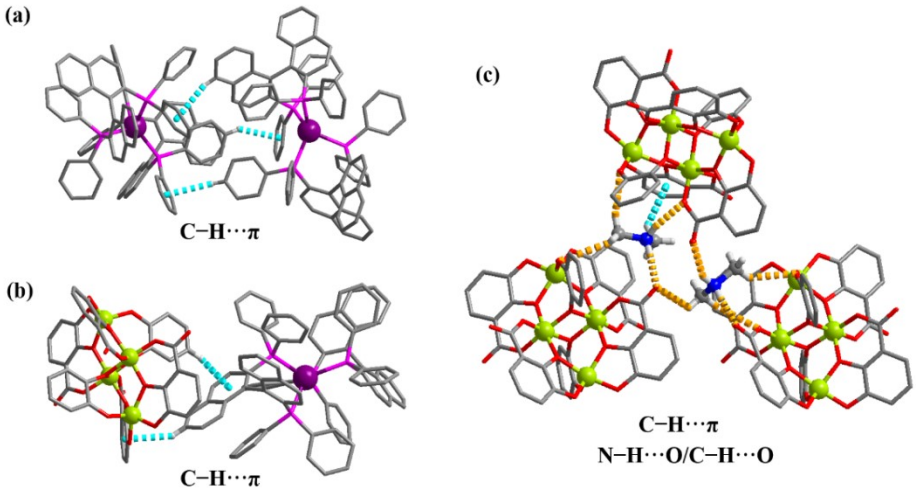

Figure S9. The supramolecular interactions in **AlOC-170(R)**.

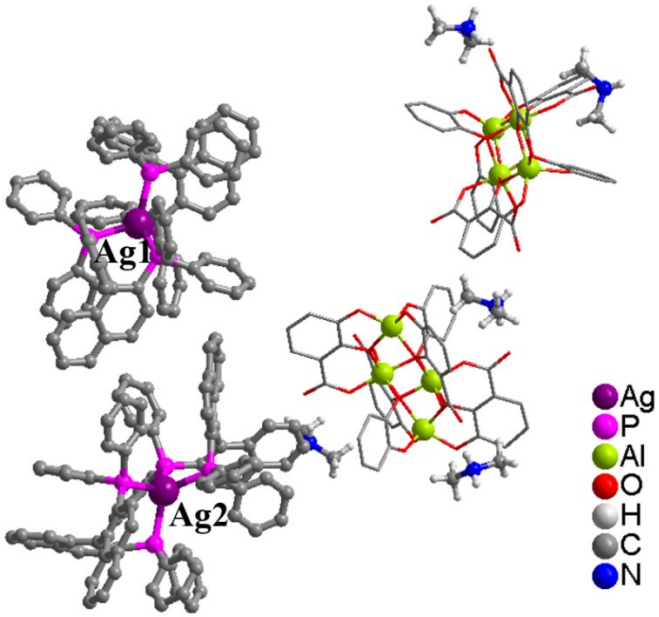

Figure S10. The asymmetric unit of **AlOC-170(S)**, showing two Al_4 clusters, two $[Ag(S\text{-}binap)_2]^+$ units, and five $(Me_2NH_2)^+$ cations. (Other $(Me_2NH_2)^+$ cation and solvent molecules could not be located because of high disorder).

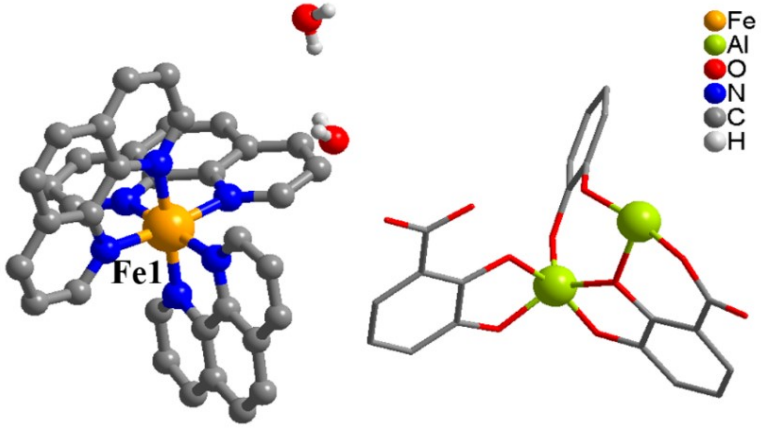

Figure S11. The asymmetric unit of **AlOC-171**, showing half of Al_4 cluster, one $[Fe(phen)_3]^{2+}$ unit, and two H_2O molecules (Other solvents could not be located because of high disorder).

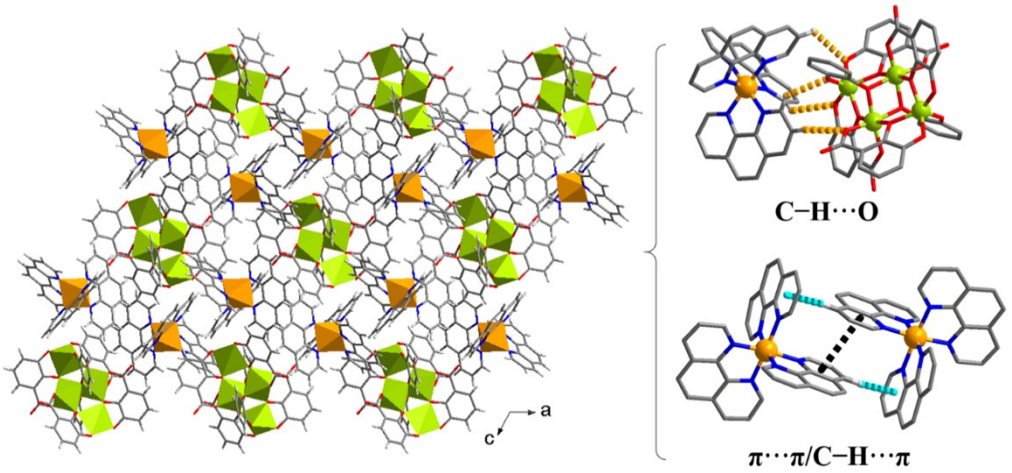

Figure S12. The packed structure along the b-axis and the supramolecular interactions in **AlOC-171**.

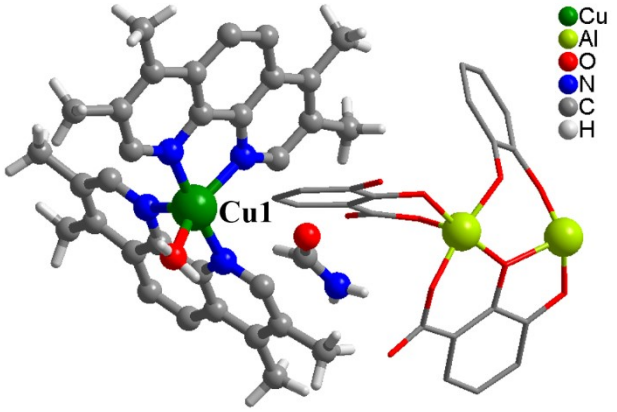

Figure S13. The asymmetric unit of **AlOC-172**, showing half of Al_4 cluster, one $[Cu(Me_4phen)_2(H_2O)]^{2+}$ unit, and one NMF molecule (Other solvents could not be located because of high disorder).

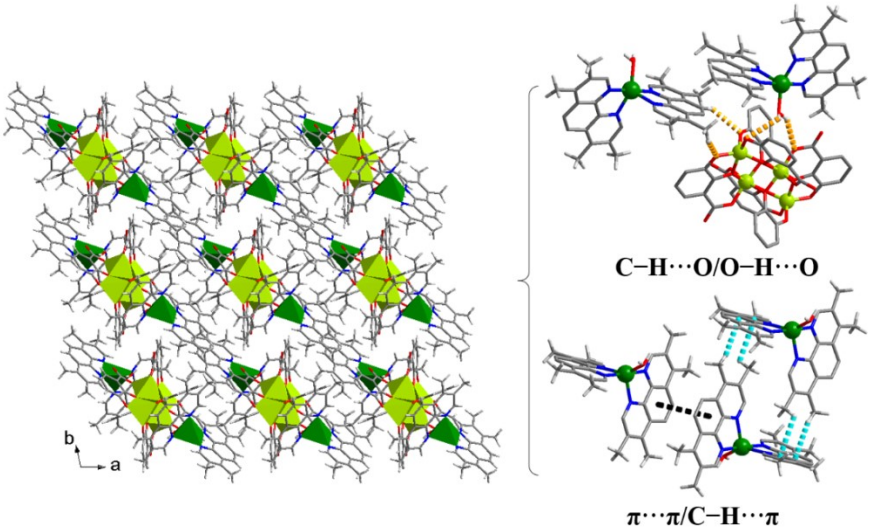

Figure S14. The packed structure along the c-axis and the supramolecular interactions in **AlOC-172**.

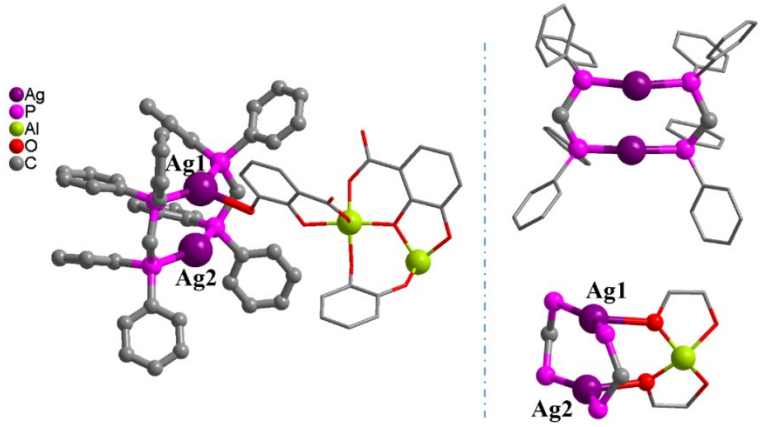

Figure S15. (Left) The asymmetric unit of **AlOC-173**, showing half of Al_4 cluster, one $[Ag_2(bdpm)_2]^{2+}$ cycle (Solvents could not be located because of high disorder). (Right) The coordination environment of Ag(Ⅰ) atoms.

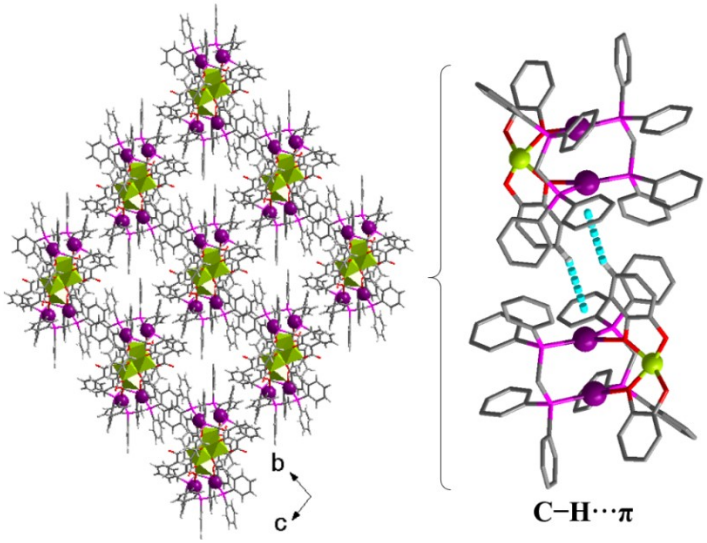

Figure S16. The packed structure along the a-axis and the supramolecular interactions in **AlOC-173**.

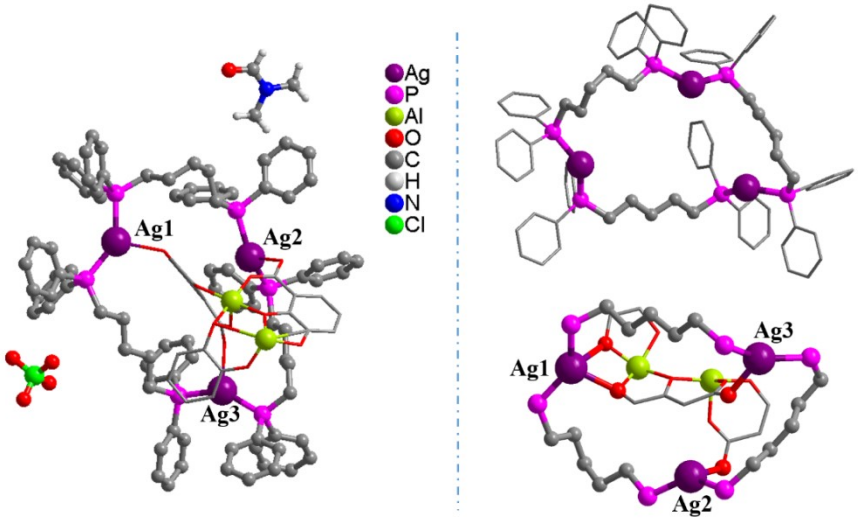

Figure S17. (Left) The asymmetric unit of **AlOC-174**, showing half of Al_4 cluster, one $[Ag_3(1,5\text{-bdpp})_3]^{3+}$ cycle, one $(ClO_4)^-$ anion and one DMF molecule (Other solvents could not be located because of high disorder). (Right) The coordination environment of Ag(Ⅰ) atoms.

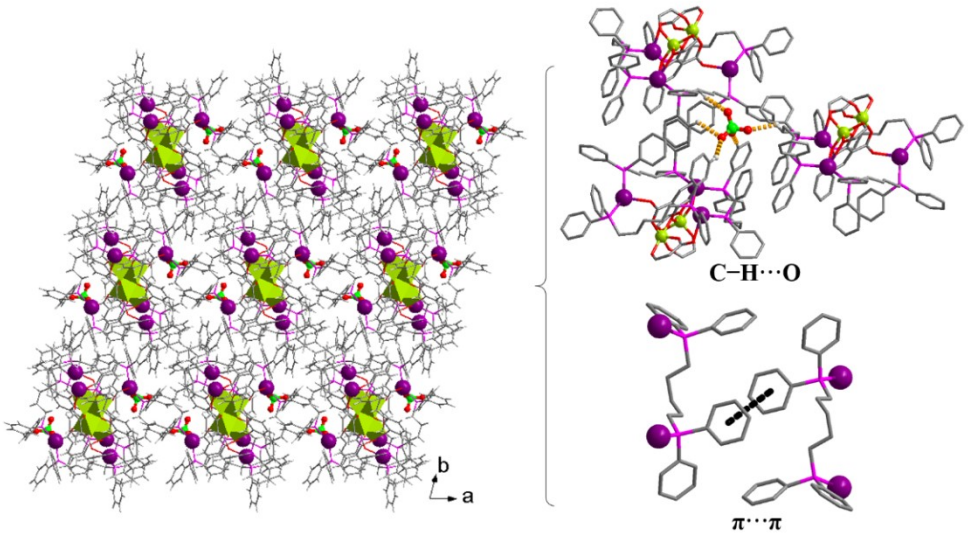

Figure S18. The packed structure along the c-axis and the supramolecular interactions in **AlOC-174**.

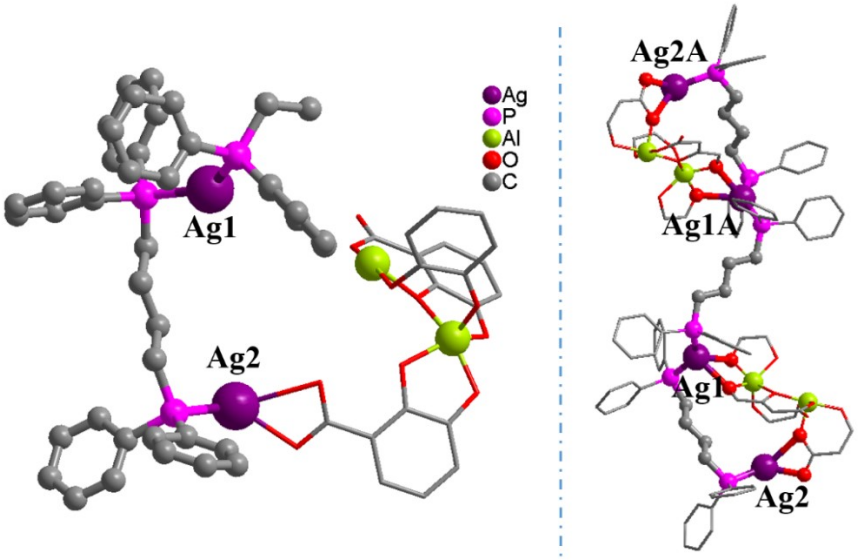

Figure S19. (Left) The asymmetric unit of **AlOC-175**, showing half of Al_4 cluster, two Ag(Ⅰ) atoms, and one and a half 1,4-bdpb ligands (Solvents could not be located because of high disorder). (Right) The coordination environment of Ag(Ⅰ) atoms.

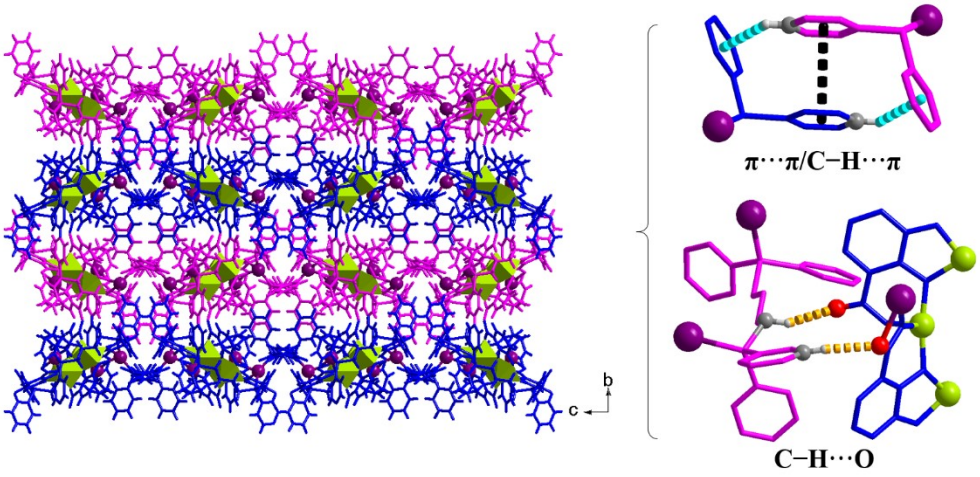

Figure S20. The packed structure along the a-axis and the interactions between adjacent chains in **AlOC-175**.

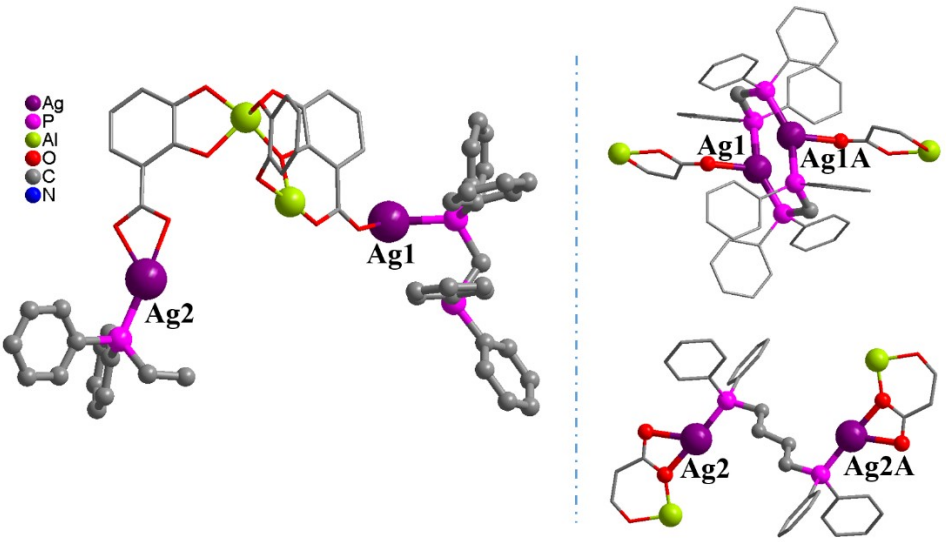

Figure S21. (Left) The asymmetric unit of **AlOC-176**, showing half of Al_4 cluster, two Ag(Ⅰ) atoms, one bdpm ligand, and half of 1,4-bdpb ligand (Solvents could not be located because of high disorder). (Right) The coordination environment of Ag(Ⅰ) atoms.

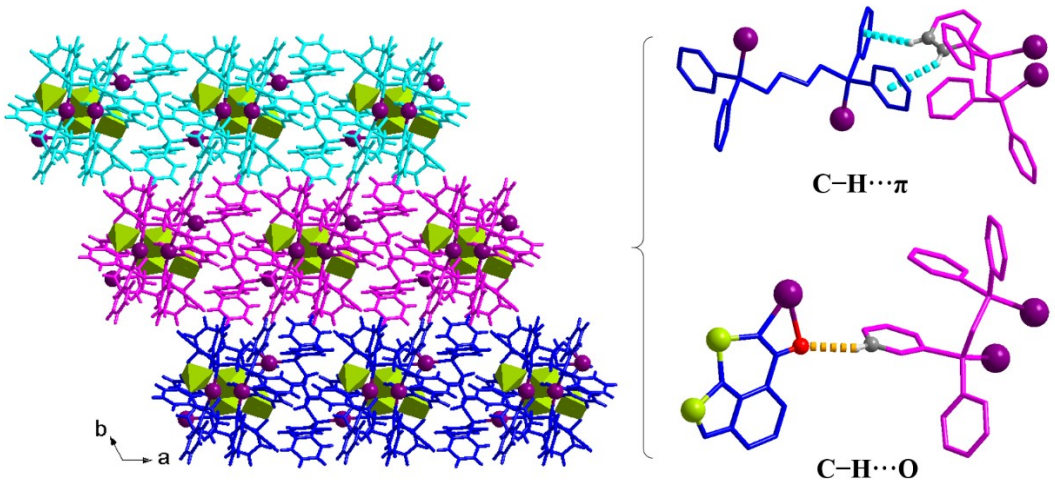

Figure S22. The packed structure along the c-axis and the interactions between adjacent layers in **AlOC-176**.

3. PXRD analyses of AlOC-168 to AlOC-176.

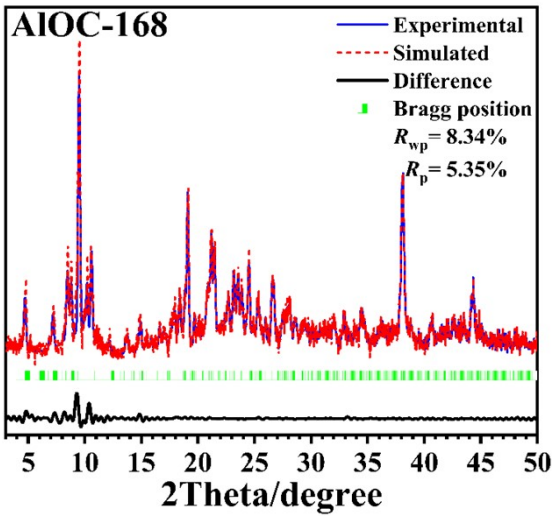

Figure S23. PXRD analyses for **AlOC-168**.

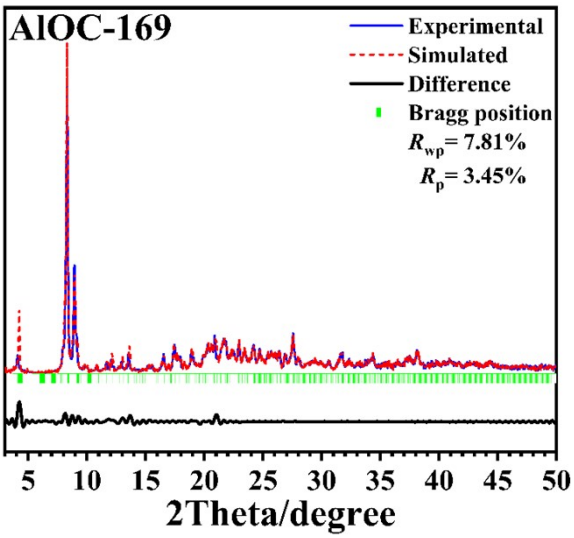

Figure S24. PXRD analyses for **AlOC-169**.

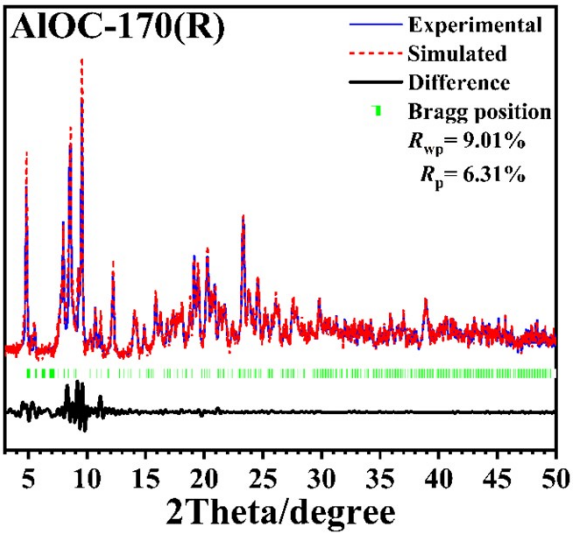

Figure S25. PXRD analyses for **AlOC-170(R)**.

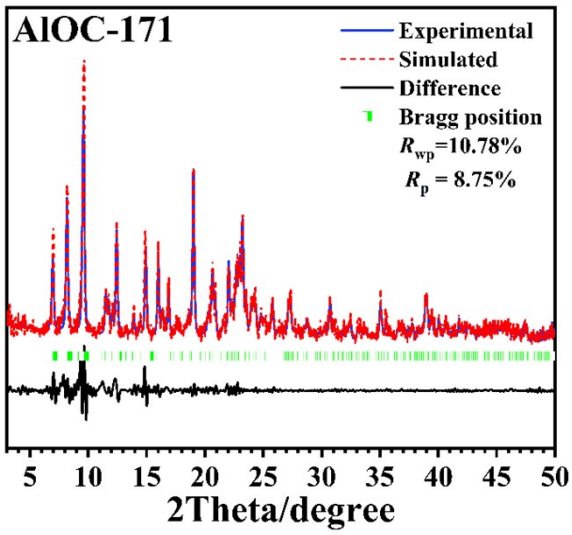

Figure S26. PXRD analyses for **AlOC-171**.

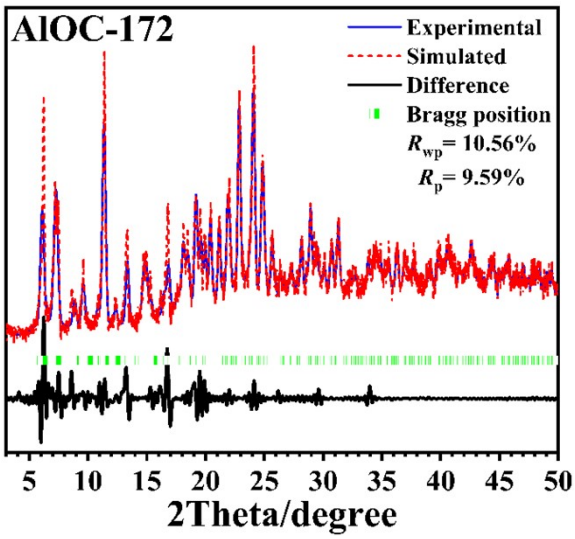

Figure S27. PXRD analyses for **AlOC-172**.

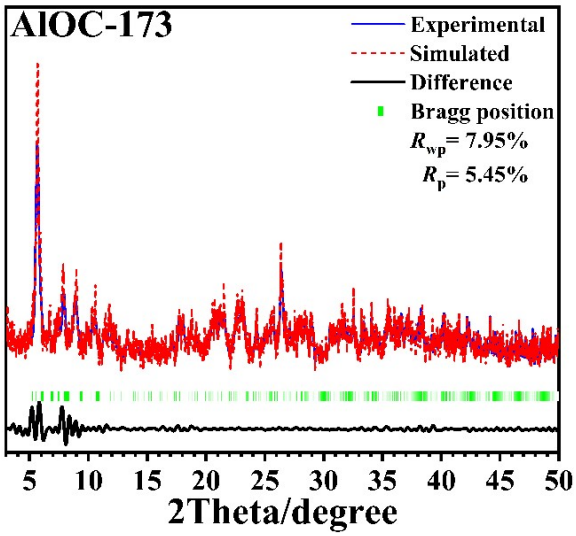

Figure S28. PXRD analyses for **AlOC-173**.

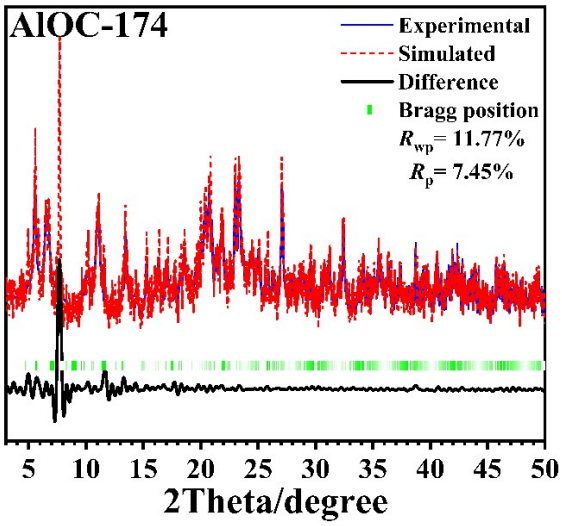

Figure S29. PXRD analyses for **AlOC-174**.

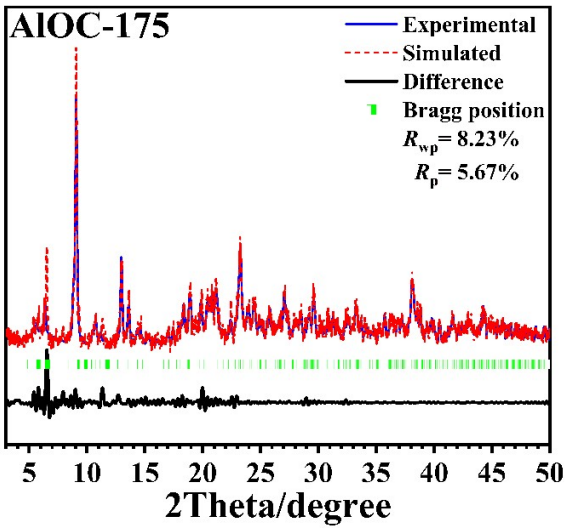

Figure S30. PXRD analyses for **AlOC-175**.

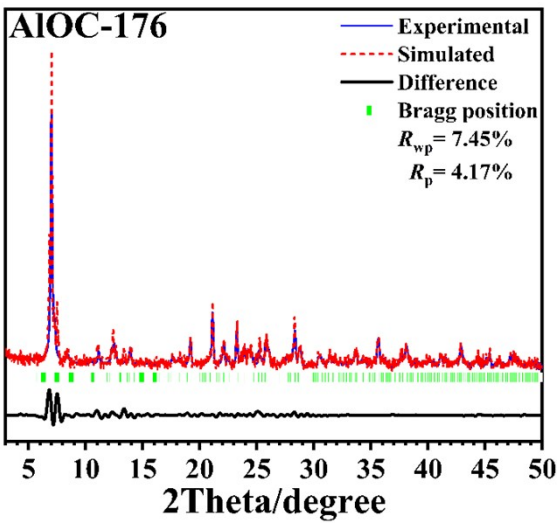

Figure S31. PXRD analyses for **AlOC-176**.

To quantitatively evaluate the degree of coincidence between experimental data

and simulated data in PXRD, we did Le Bail fits for all structures (Figures S23-S31). In Le Bail fit, the most important data are R_{wp} and R_p. If R_{wp} and R_p are both < 10 %, or one of them < 10 %, the other is close to 10 %, it means the degree of coincidence between experimental data and simulated data is good, and the phase purity is pretty good. As shown in Figures S23-S31, nearly R_{wp} and R_p in all structures are in line with the above criteria, indicating that these compounds have high phase purity.

4. The TGA curves of AlOC-168 to AlOC-176.

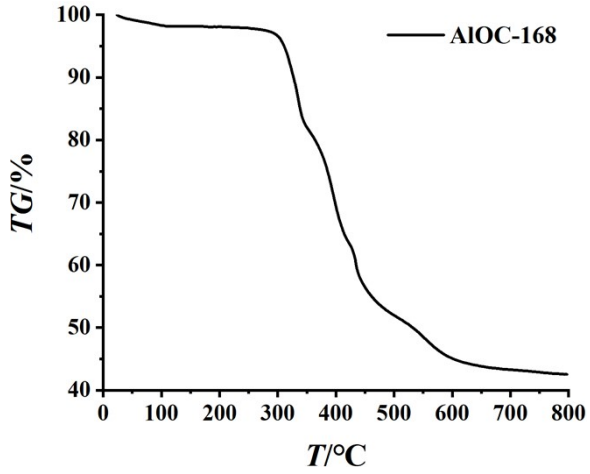

Figure S32. The TGA curve of **AlOC-168**.

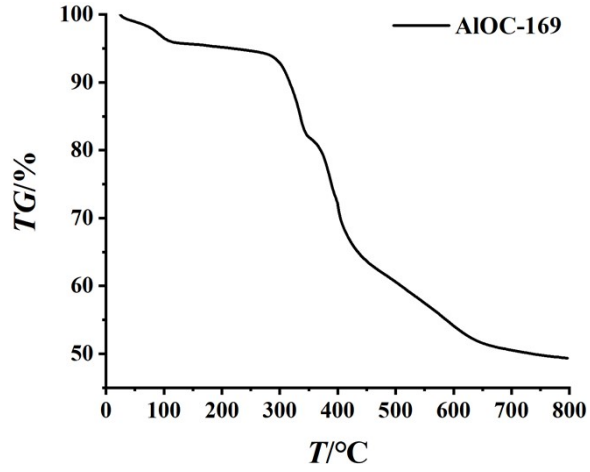

Figure S33. The TGA curve of **AlOC-169**.

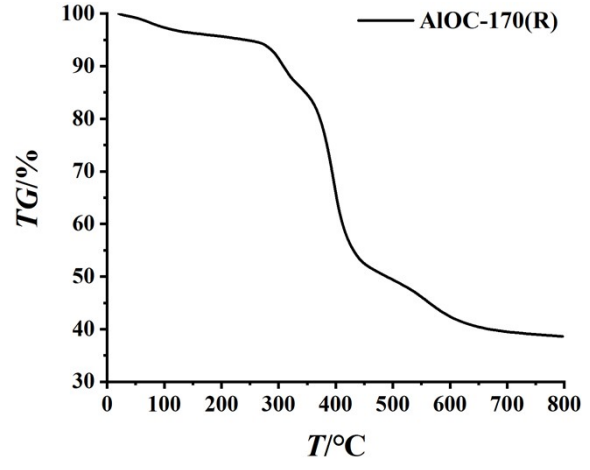

Figure S34. The TGA curve of **AlOC-170(R)**.

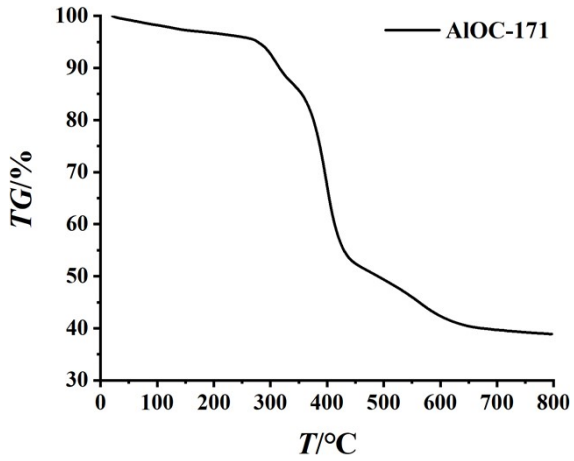

Figure S35. The TGA curve of **AlOC-171**.

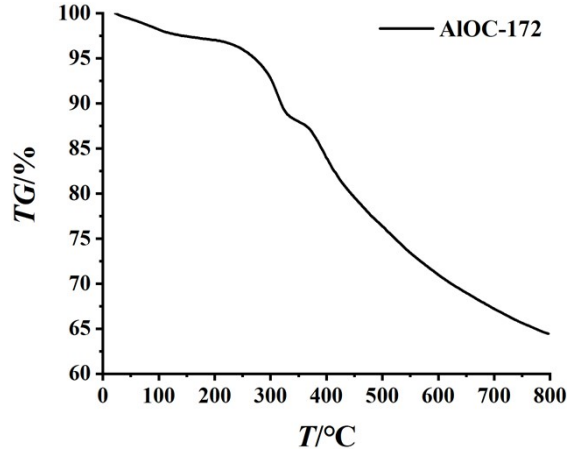

Figure S36. The TGA curve of **AlOC-172**.

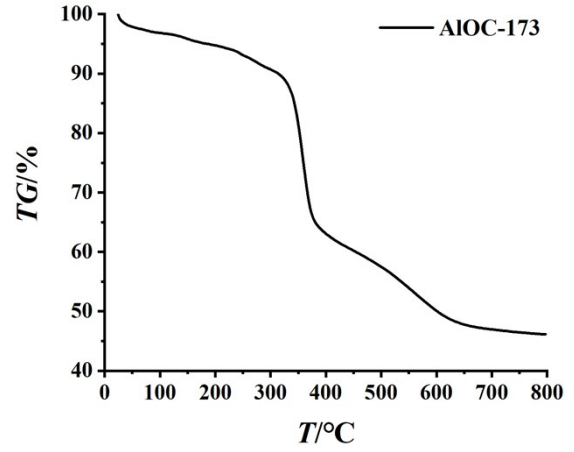

Figure S37. The TGA curve of **AlOC-173**.

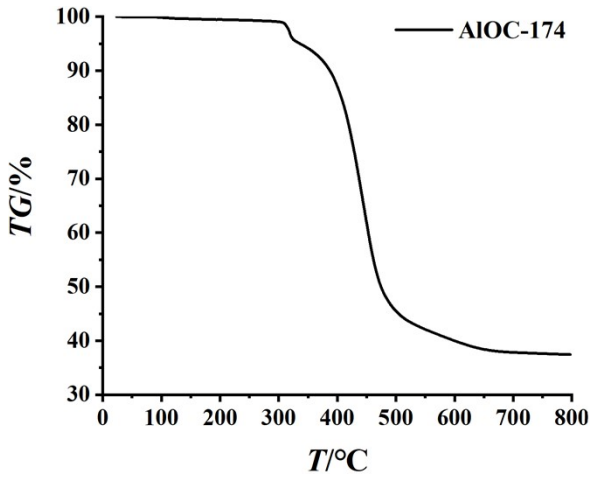

Figure S38. The TGA curve of **AlOC-174.**

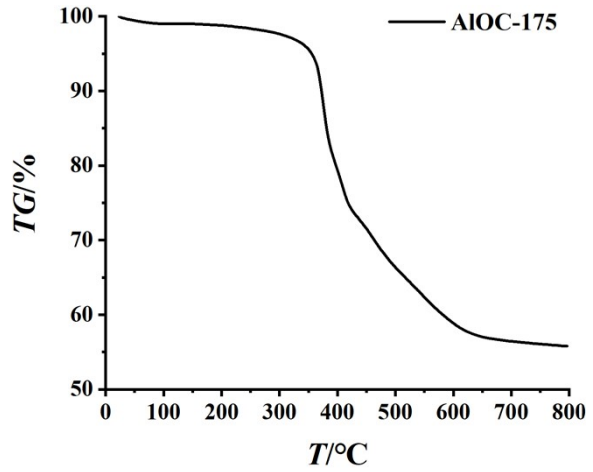

Figure S39. The TGA curve of **AlOC-175**.

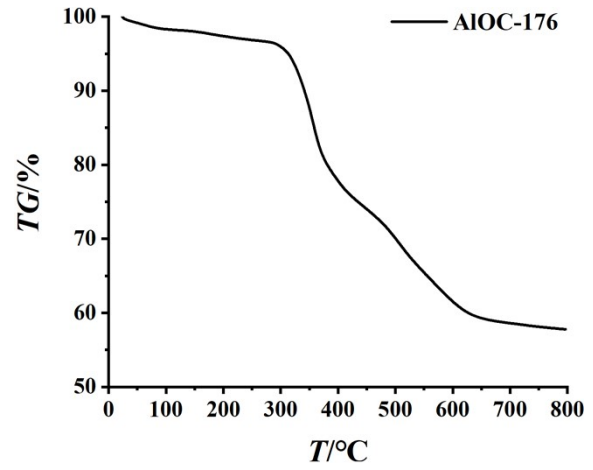

Figure S40. The TGA curve of **AlOC-176**.

TGA curves of **AlOC-168-176** were carried out from room temperature to 800 °C with a heating speed of 10 °C/min in a flowing N_2 atmosphere (Figures S32-S40).

Except for **AIOC-174** (no apparent weight loss), all the samples have a small weight loss before 110 °C, which is related to the removal of EtOH and H_2O or H_2O (for **AIOC-172**) molecules (lower boiling point). It is clear that there is almost no obvious weight loss from 110-250 °C, indicating that DMF or NMF (high boiling point) are not present in their structure. The above results show that there are a few solvent molecules in the structure of these compounds, which further indicates that their supramolecular packing structures are dense. Around 300 °C, these compounds began to decompose, and the residues may be Al_2O_3, AgO or Fe_2O_3 and CuO, etc.

5. The UV/Vis absorption spectra of Al_4 precursor and compounds AlOC-168 to AlOC-176.

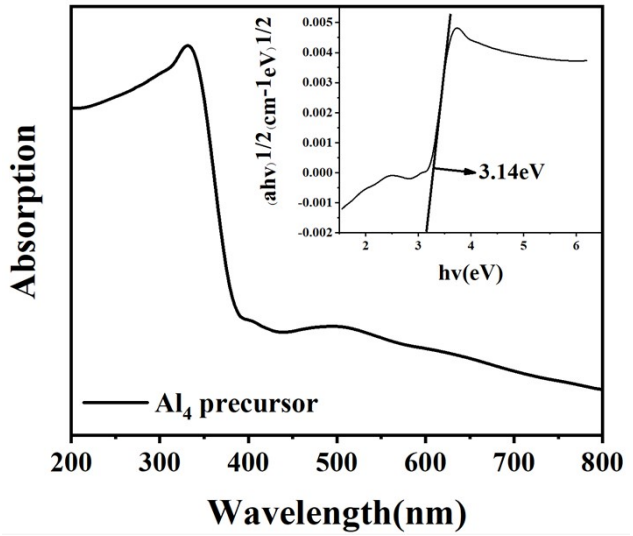

Figure S41. The solid-state absorption spectra of Al_4 precursor.

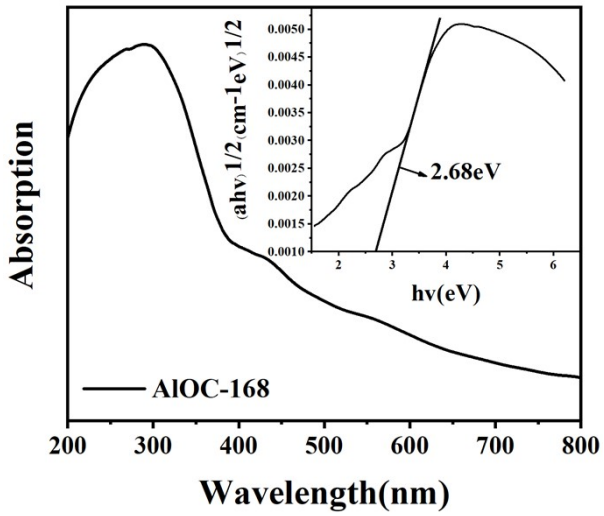

Figure S42. The solid-state absorption spectra of **AlOC-168**.

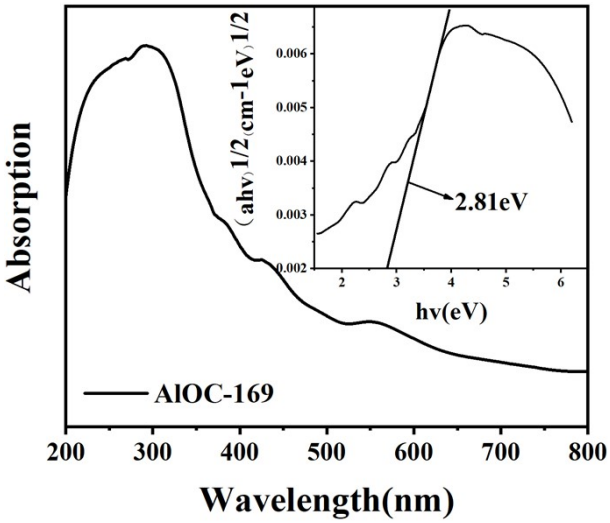

Figure S43. The solid-state absorption spectra of **AlOC-169**.

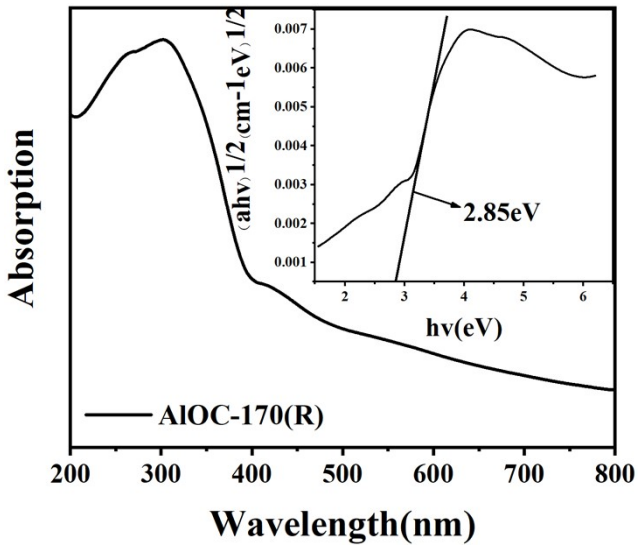

Figure S44. The solid-state absorption spectra of **AlOC-170(R)**.

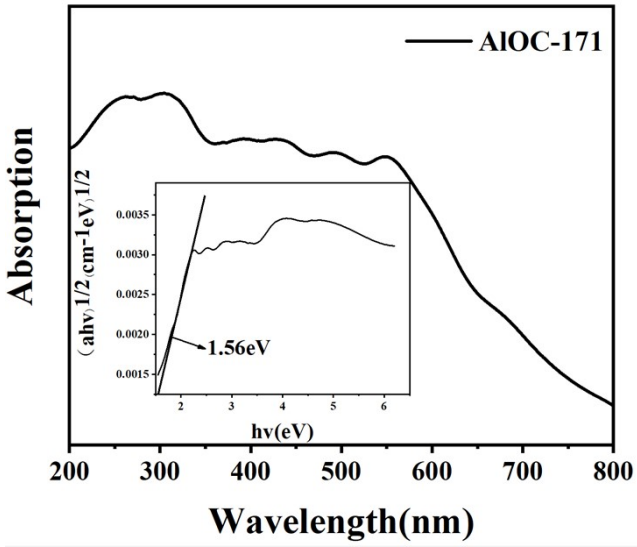

Figure S45. The solid-state absorption spectra of **AlOC-171**.

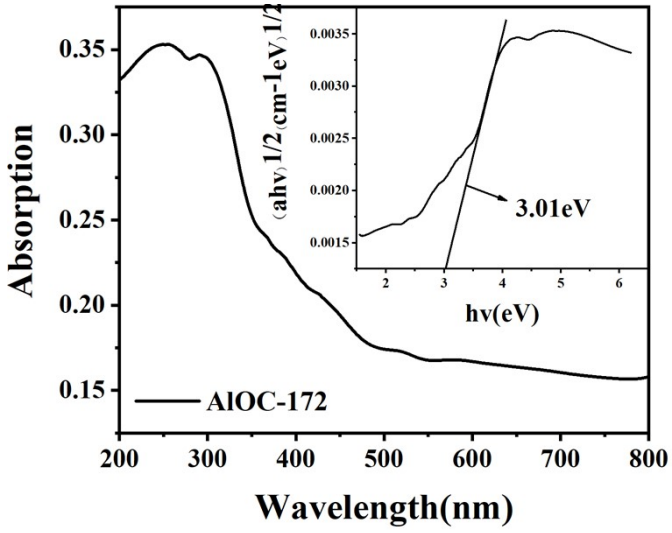

Figure S46. The solid-state absorption spectra of **AlOC-172**.

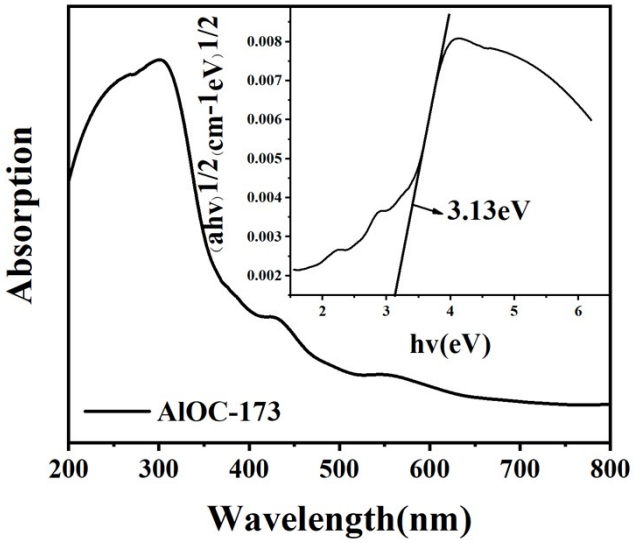

Figure S47. The solid-state absorption spectra of **AlOC-173**.

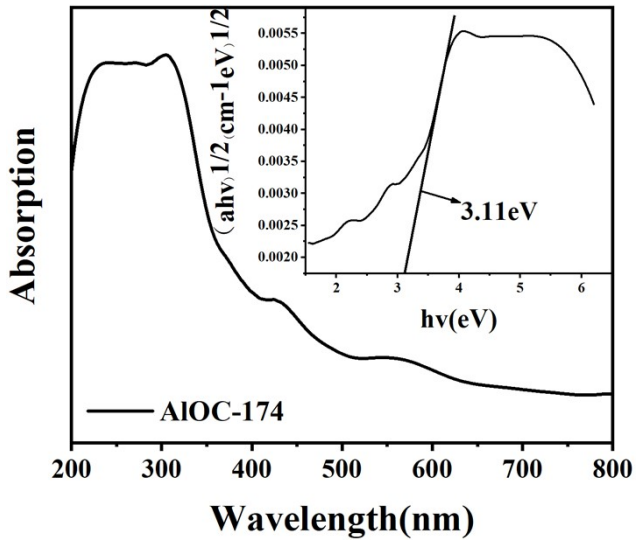

Figure S48. The solid-state absorption spectra of **AlOC-174**.

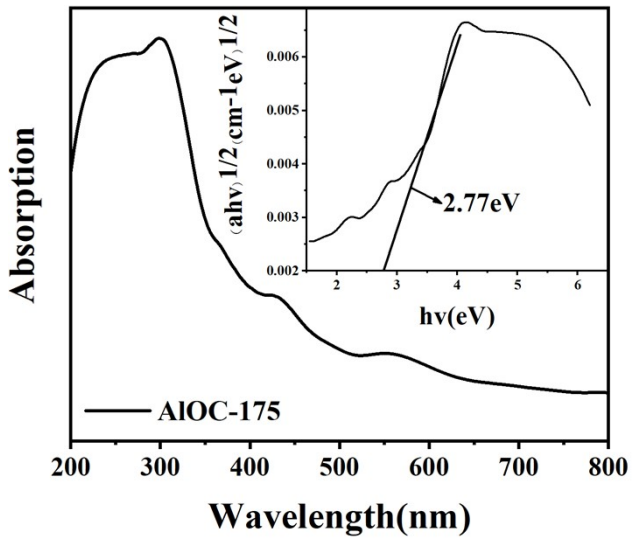

Figure S49. The solid-state absorption spectra of **AlOC-175**.

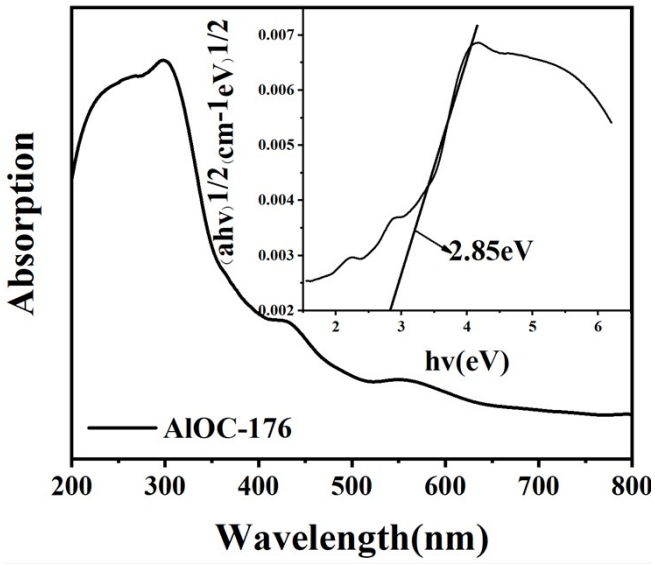

Figure S50. The solid-state absorption spectra of **AlOC-176**.

6. The EDS spectra of AlOC-168 to AlOC-176.

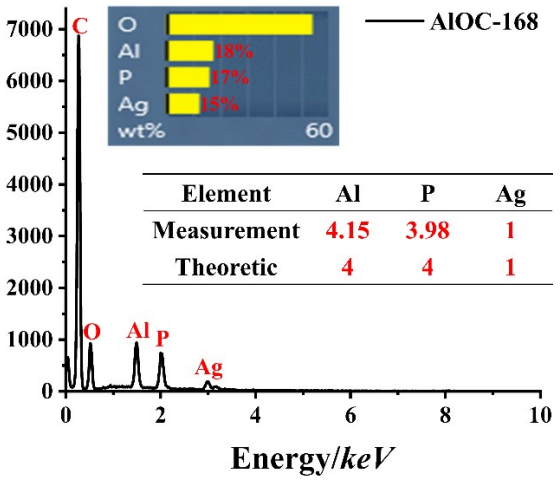

Figure S51. The EDS spectra of **AlOC-168**.

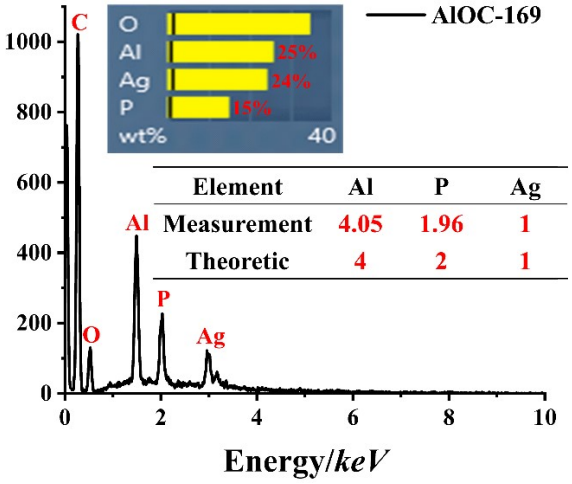

Figure S52. The EDS spectra of **AlOC-169**.

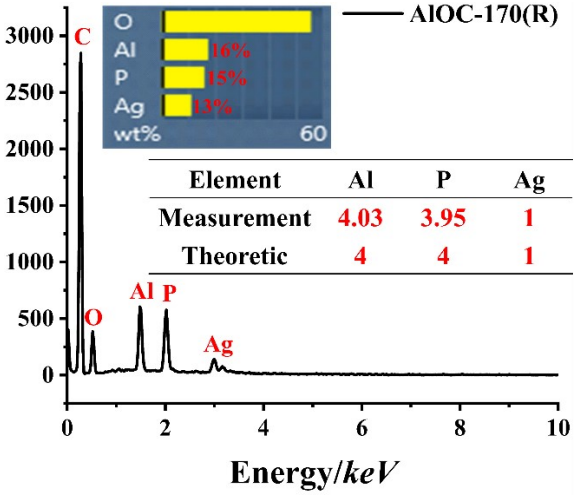

Figure S53. The EDS spectra of **AlOC-170**.

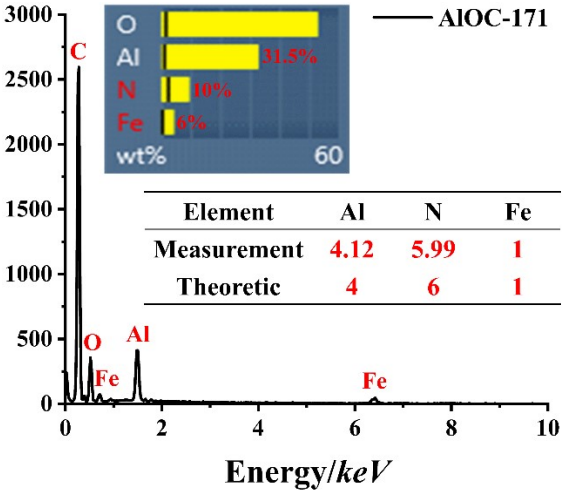

Figure S54. The EDS spectra of **AlOC-171**.

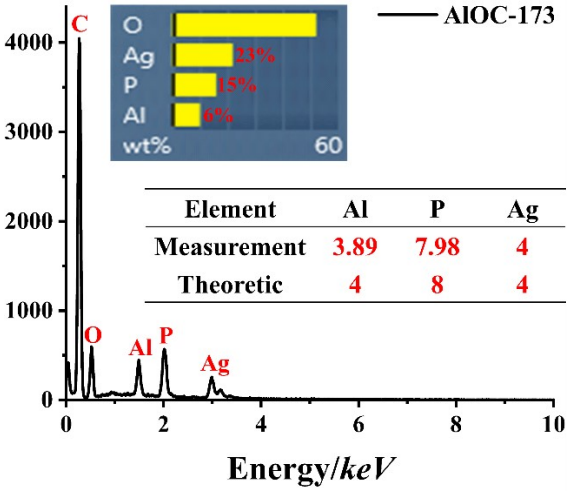

Figure S55. The EDS spectra of **AlOC-173**.

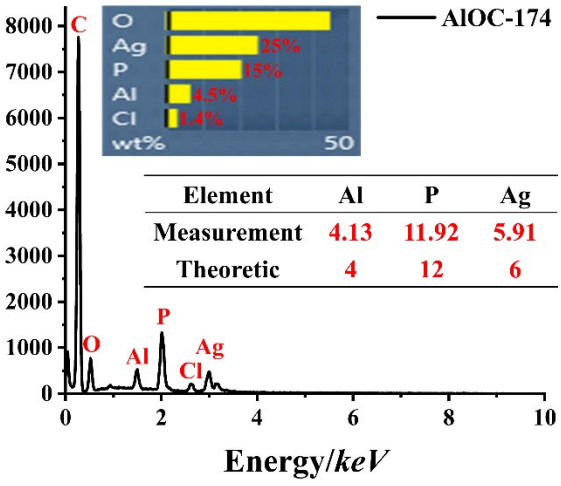

Figure S56. The EDS spectra of **AlOC-174**.

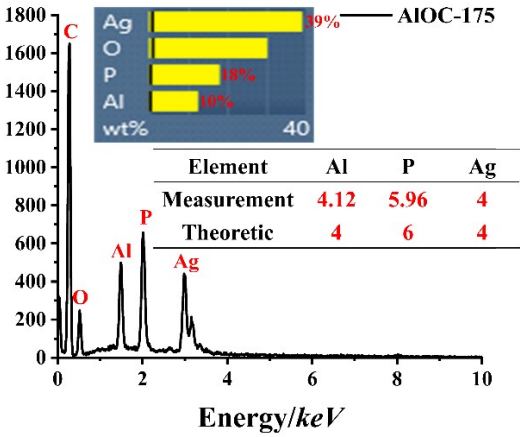

Figure S57. The EDS spectra of **AlOC-175**.

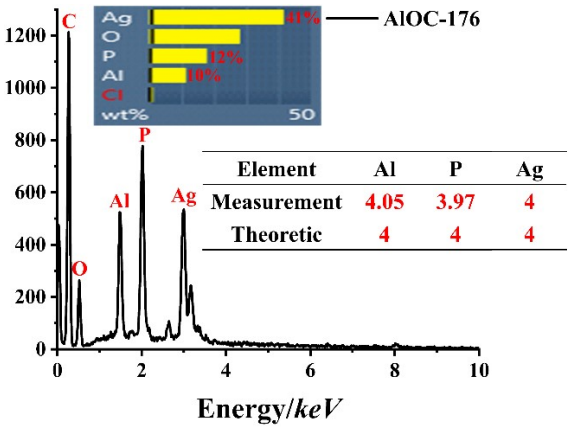

Figure S58. The EDS spectra of **AlOC-176**.

From the EDS data of these compounds, the elements (mainly Al, P, Ag) are also analyzed in detail. By calculation, the mass percentage (Wt %) of these elements is converted to the atomic ratio, as shown in Figures S51-S58. The results show that the atomic ratio of Al, P, and Ag elements is almost consistent with the theoretical (obtained from single crystal structure data), which further indicates the high purity of these samples.

7. The Fluorescence Property.

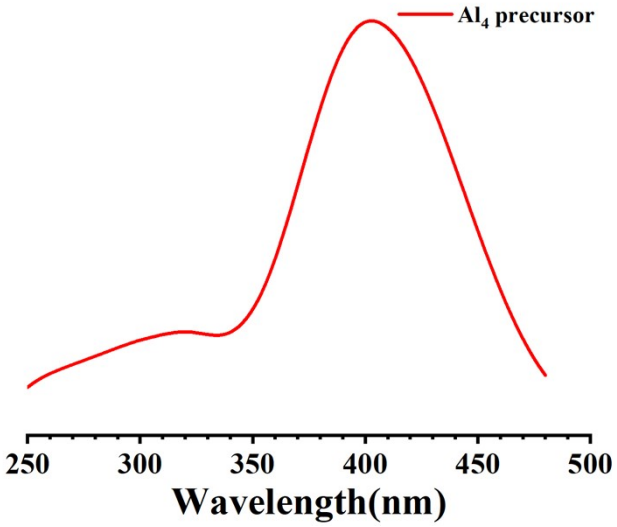

Figure S59. The excitation spectrum of Al_4 precursor.

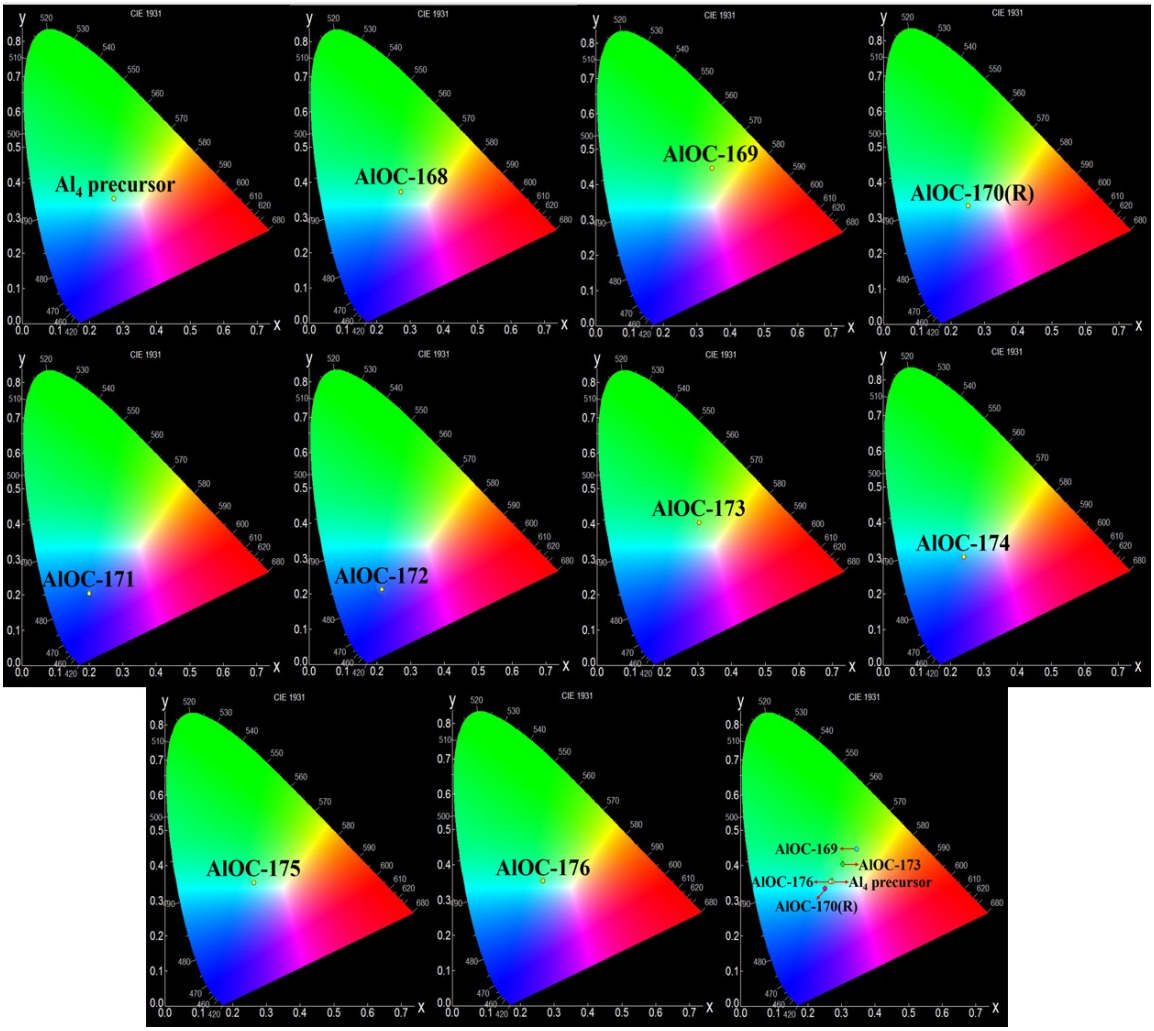

Figure S60. The CIE coordinates of Al_4 precursor and compounds **AlOC-168** to **AlOC-176**.

8. CD spectra.

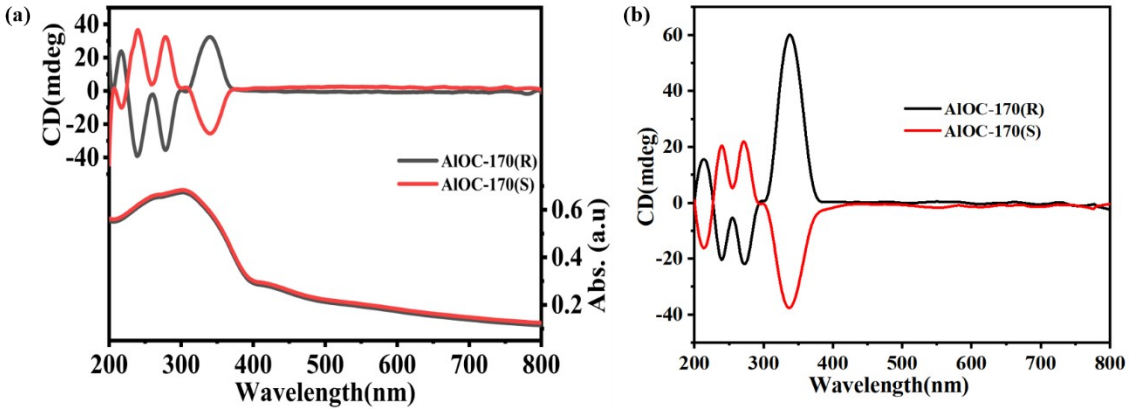

Figure S61. (a) CD spectra of AIOC-170(R) and AIOC-170(S) in methanol and UV-vis spectra of AIOC-170(R) and AIOC-170(S) in solid-state. (b) Solid-state CD spectra for **AIOC-170(R)** and **AIOC-170(S)**.

9. IR spectrum.

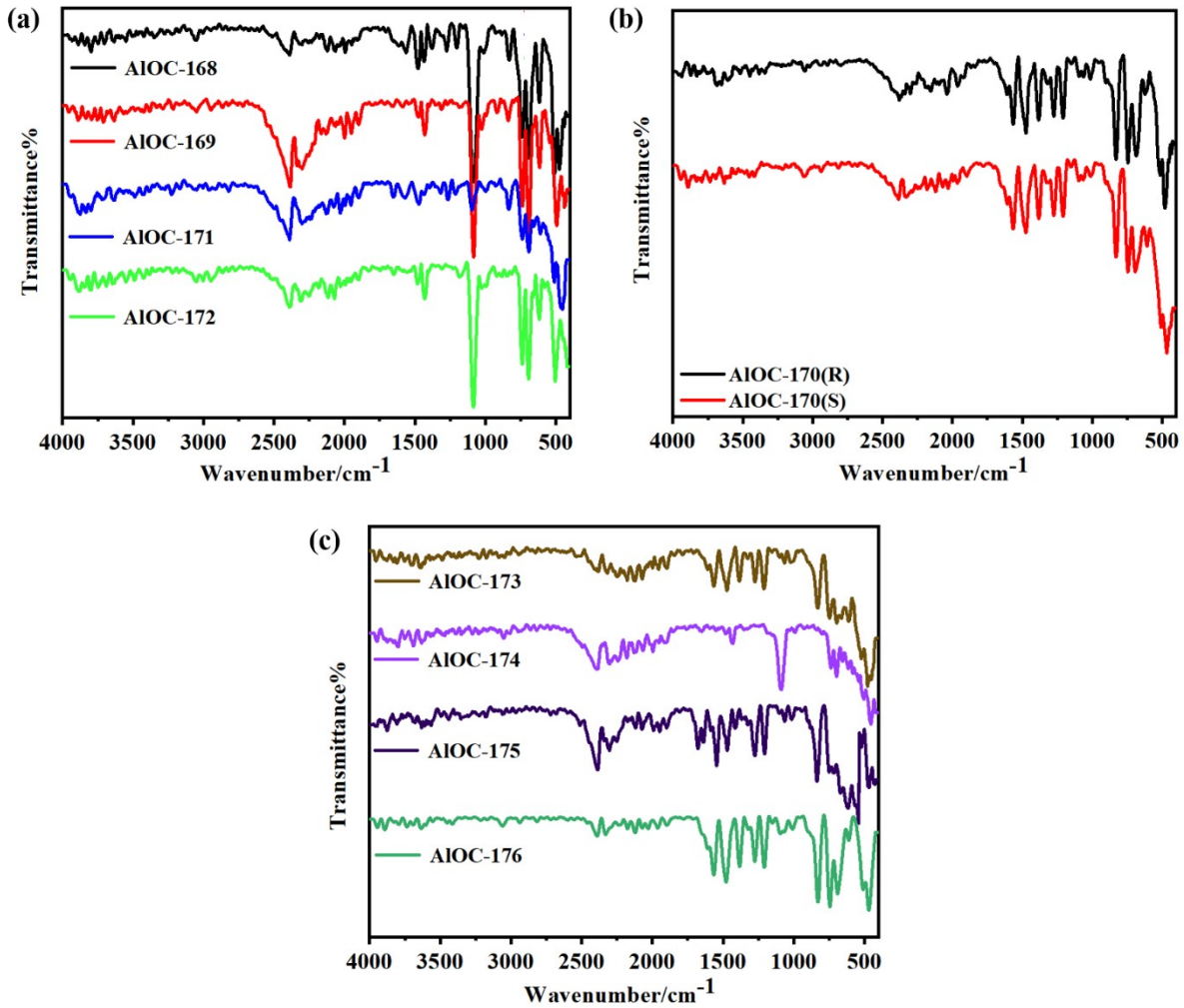

Figure S62. IR spectrum of **AlOC168-176**.

The vibrations near 3050 cm^{-1} are attributed to C-H stretching in aromatic rings. The band at 1550 cm^{-1} corresponds to asymmetric stretching of carboxylate groups. Symmetric stretching of carboxylate groups is observed at 1420 cm^{-1}. The vibration at 1090 cm^{-1} is ascribed to C-N vibrations in the dimethylamine guest molecule.This confirms the structural accuracy.

10. The NLO Property.

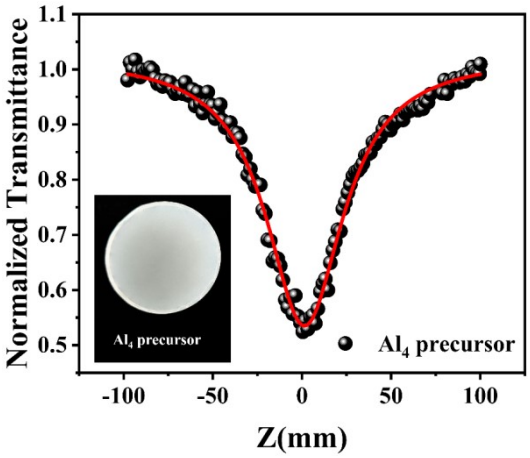

Figure S63. The Z-scan curve of Al_4 precursor.

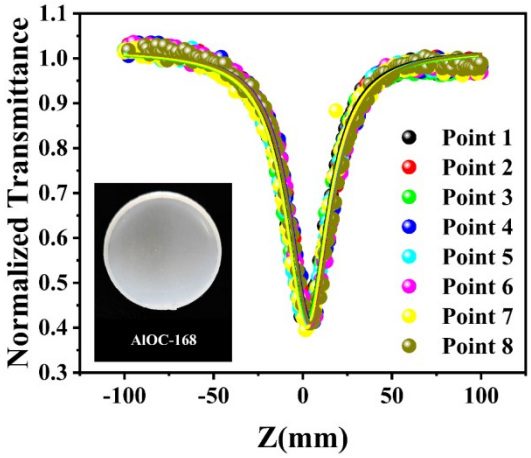

Figure S64. The Z-scan curve of **AlOC-168**.

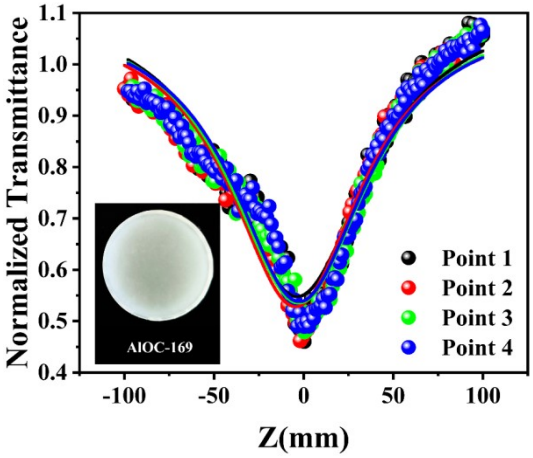

Figure S65. The Z-scan curve of **AlOC-169**.

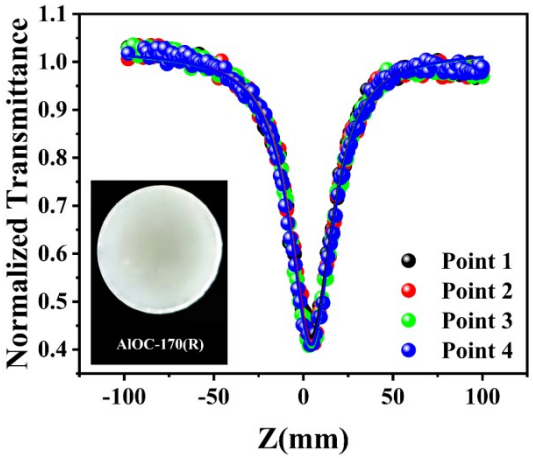

Figure S66. The Z-scan curve of **AIOC-170(R)**.

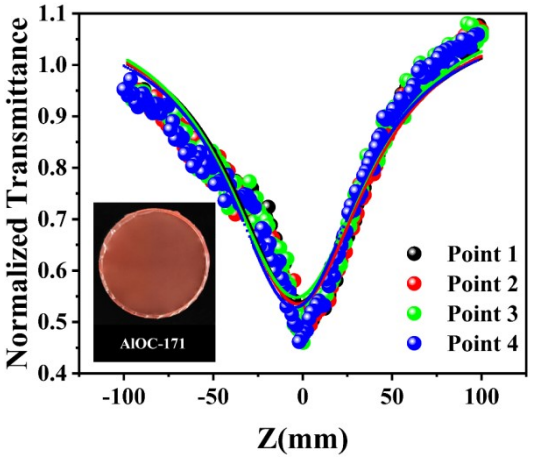

Figure S67. The Z-scan curve of **AIOC-171**.

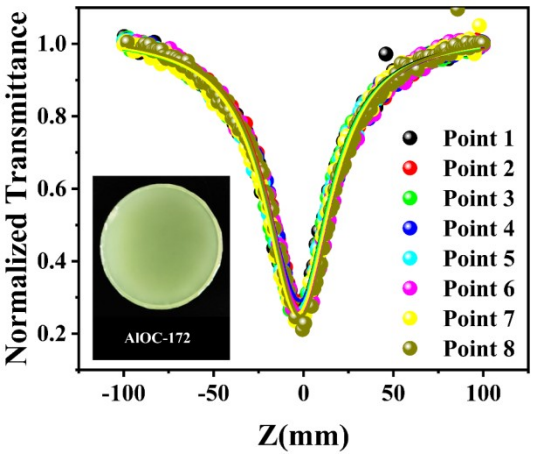

Figure S68. The Z-scan curve of **AIOC-172**.

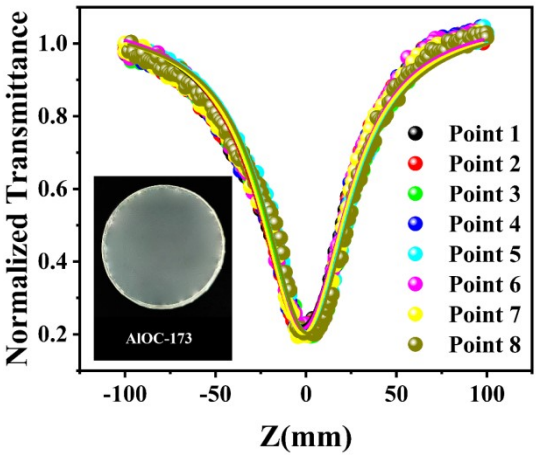

Figure S69. The Z-scan curve of **AIOC-173**.

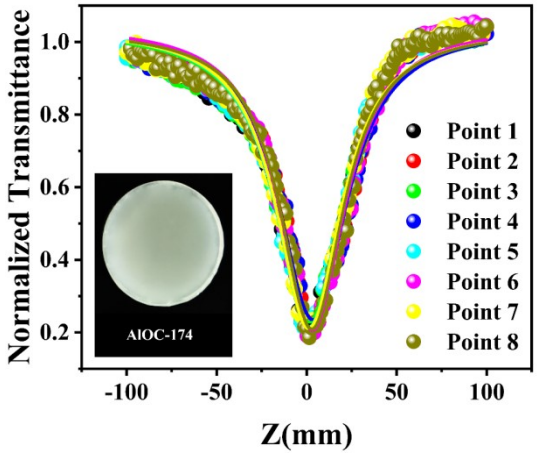

Figure S70. The Z-scan curve of **AIOC-174**.

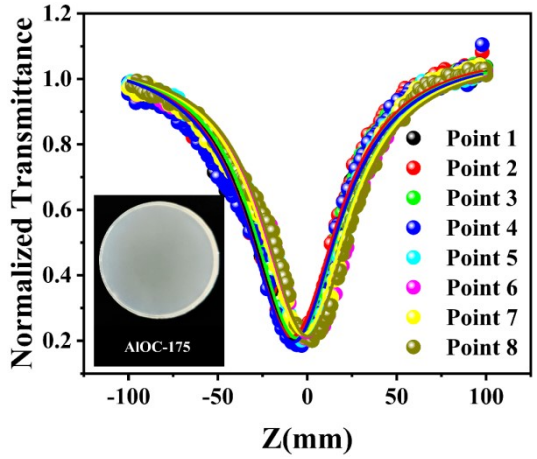

Figure S71. The Z-scan curve of **AIOC-175**.

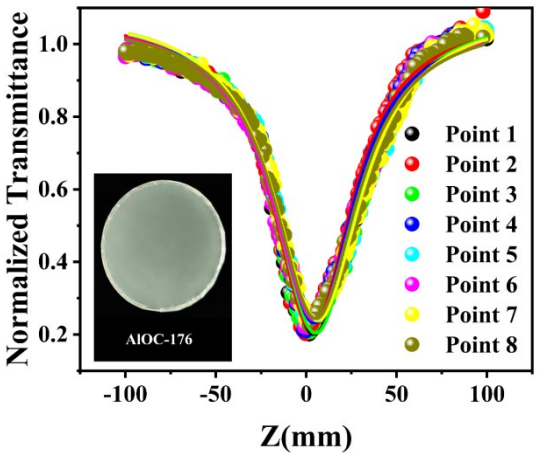

Figure S72. The Z-scan curve of **AIOC-176**.

Table S4. The third-order nonlinear optical parameters of compounds Al_4 precursor and **AIOC-168** to **AIOC-176**.

Samples	T/%	β(cm/GW)	T_{min}	F_{OL}(J/cm^2)
Al_4 precursor	70	98	0.51	5.12
AIOC-168	70	200	0.38	1.09
AIOC-169	70	120	0.44	3.45
AIOC-170(R)	70	220	0.40	1.23
AIOC-171	70	130	0.45	3.59
AIOC-172	70	700	0.23	0.61
AIOC-173	70	750	0.19	0.39
AIOC-174	70	730	0.21	0.86
AIOC-175	70	710	0.17	0.75
AIOC-176	70	700	0.18	0.33

Table S5. The comparison of the nonlinear absorption coefficients between this work and other work.

Samples	Nonlinear absorption coefficient *β* (cm/GW)	References
Al_4 precursor	**98**	This work
AIOC-168	**200**	This work
AIOC-169	**120**	This work

AIOC-170(R)	**220**	This work
AIOC-171	**130**	This work
AIOC-172	**700**	This work
AIOC-173	**750**	This work
AIOC-174	**730**	This work
AIOC-175	**710**	This work
AIOC-176	**700**	This work
AIOC-50	1182	*Angew. Chem. Int. Ed. 2021, 60, 4849.*
AIOC-52	4384	*Angew. Chem. Int. Ed. 2021, 60, 4849.*
AIOC-57	8500	*Chem. Commun. 2021,57,12820.*
AIOC-76	0.61	*Angew. Chem. Int. Ed. 2022, 61, 202116563.*
AIOC-90	13.5	*Aggregate 2022, e264.*
AIOC-91	21.2	*Aggregate 2022, e264.*
AIOC-92	7.5	*Aggregate 2022, e264.*
AIOC-93	71.8	*Aggregate 2022, e264.*
AIOC-94	41.2	*Aggregate 2022, e264.*
AIOC-95	48.5	*Aggregate 2022, e264.*
PTC-273	11700	*Aggregate 2022, e264.*
PTC-274	2410	*J. Am. Chem. Soc. 2022, 144, 8153.*
PTC-296	-160	*J. Am. Chem. Soc. 2022, 144, 8153.*
$AgSn_{12}$	2550	*Inorg. Chem. Front. 2022, 9, 1984.*
Cu_8	350	*Angew. Chem. Int. Ed. 2022, 61, 202202853.*
Cage-1	7.5	*Chem. Eur. J. 2018, 24, 19317.*
Cage-2	3.2	*J. Am. Chem. Soc. 2020, 142, 13356.*
Cage-3	3.4	*J. Am. Chem. Soc. 2020, 142, 13356.*
ZnTPyP-1(Zn/Zn)/PDMS	1350	*J. Am. Chem. Soc. 2020, 142, 13356.*
ZnTPyP-2/PDMS	400	*J. Am. Chem. Soc., 2021, 143, 17162–17169.*
TPyP(Zn)/PDMS	200	*J. Am. Chem. Soc., 2021, 143, 17162–17169.*
TPyP(Mn)/PDMS	160	*J. Am. Chem. Soc., 2021, 143, 17162–17169.*